

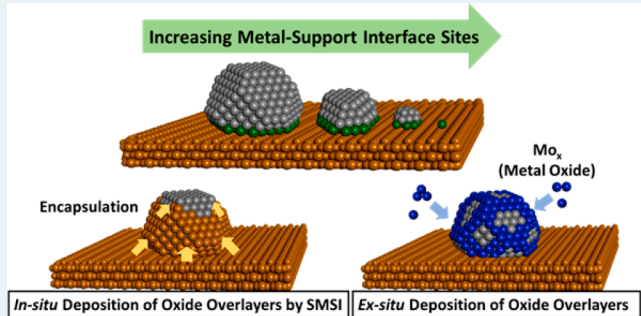
Approaches for Understanding and Controlling Interfacial Effects in Oxide-Supported Metal Catalysts

Insoo Ro, Joaquin Resasco, and Phillip Christopher*

Department of Chemical Engineering, University of California, Santa Barbara, Santa Barbara, California 93117, United States

ABSTRACT: Heterogeneous supported metal catalysts are critical for a wide range of chemical conversion technologies. While the fundamental properties of extended metal surfaces are well understood and active sites on such systems can be designed for targeted applications, much less is known about the properties of active sites formed at the interface of nanometer-scale metal structures and their underlying oxide support. The goal of this Perspective is to highlight recent progress in understanding and controlling metal–oxide support interfacial sites on high-surface-area catalysts. Focus is given to how metal particle size, support migration onto metal particles, and intentional deposition of oxides on metal particles can be used to create high concentrations of interfacial sites. The impact of interface formation on properties of nearby metal and oxide sites is discussed in the context of understanding if the uniqueness of interfacial sites stems from bifunctionality, or if the distinct electronic properties of atoms near the interface control their catalytic behavior. Furthermore, the importance of structural dynamics of interfaces is highlighted. We pay particular attention to how microscopy, spectroscopy, and theory can be used in concert to provide insights into the behavior of these systems. We end with a forward-looking discussion on the frontiers in this field and the potential for directing catalytic reactivity by controlling the quantity and nature of metal–support interfaces.

KEYWORDS: supported metal catalysts, support effects, interface, spectroscopy, microscopy



1. INTRODUCTION

The fuel, commodity chemical, and automotive industries have relied on supported metals catalysts for decades to drive chemical conversions because of their high reactivity, selectivity, and stability in many industrially important reactions. A majority of supported metal catalysts used industrially and studied in research settings prior to the 1970s exploited nontransition metal oxides (e.g., Al₂O₃, SiO₂) as supports.¹ Nontransition metal oxide supports are characterized by stable O²⁻ ions and uncommon formation of metal–metal bonds.² Interactions between these supports and active metal species rarely involve significant charge transfer or participation of support lattice oxygen in the catalytic cycle.^{2,3} While the catalytic reactivity of these materials can be influenced by the inherent acidity or basicity of the oxide, the support primarily acts as a high-surface area and thermally stable material that disperses metal species as nanometer-scale particles, allowing for high metal surface area to volume ratios and high active site densities in packed bed reactors.^{4,5}

During the 1970s, observations suggested that when metallic nanoparticles are supported on transition metal oxides (TiO₂, Nb₂O₅, CeO₂, etc.), they display tunable chemical and catalytic behavior.⁶ The differentiating features of transition metal oxides, as compared with nontransition metal oxide supports, are their reducibility and capacity for metal–metal bonding.²

Following initial reports that examined the behavior of supported Pt-group metal nanoparticles on transition metal oxides, it was quickly identified that the support composition and pretreatment conditions could strongly influence chemical and catalytic behavior.^{1,6–9} These findings led to an explosion of research into the broad area of metal–support interactions, with focus on understanding how active metal structures and supports physically and chemically influence each other and how these influences can be controlled to manipulate the catalytic properties of supported metals.

Specific interactions between catalytically active metals and the supports they are dispersed on have been associated with a wide range of physical and chemical observations, which influence the catalytic activity, selectivity, and stability of supported catalysts. For example, supports with engineered characteristics have been shown to stabilize low nuclearity metal species by minimizing atom diffusion,^{10–14} controlling active metal geometry,^{15–20} modifying active metal electronic structure via charge transfer,²¹ and directing mass transfer at active metal sites through the use of porous supports.²² In addition to supports modifying the properties of supported metals, it has also been demonstrated that metals can increase

Received: May 28, 2018

Revised: June 29, 2018

Published: July 3, 2018

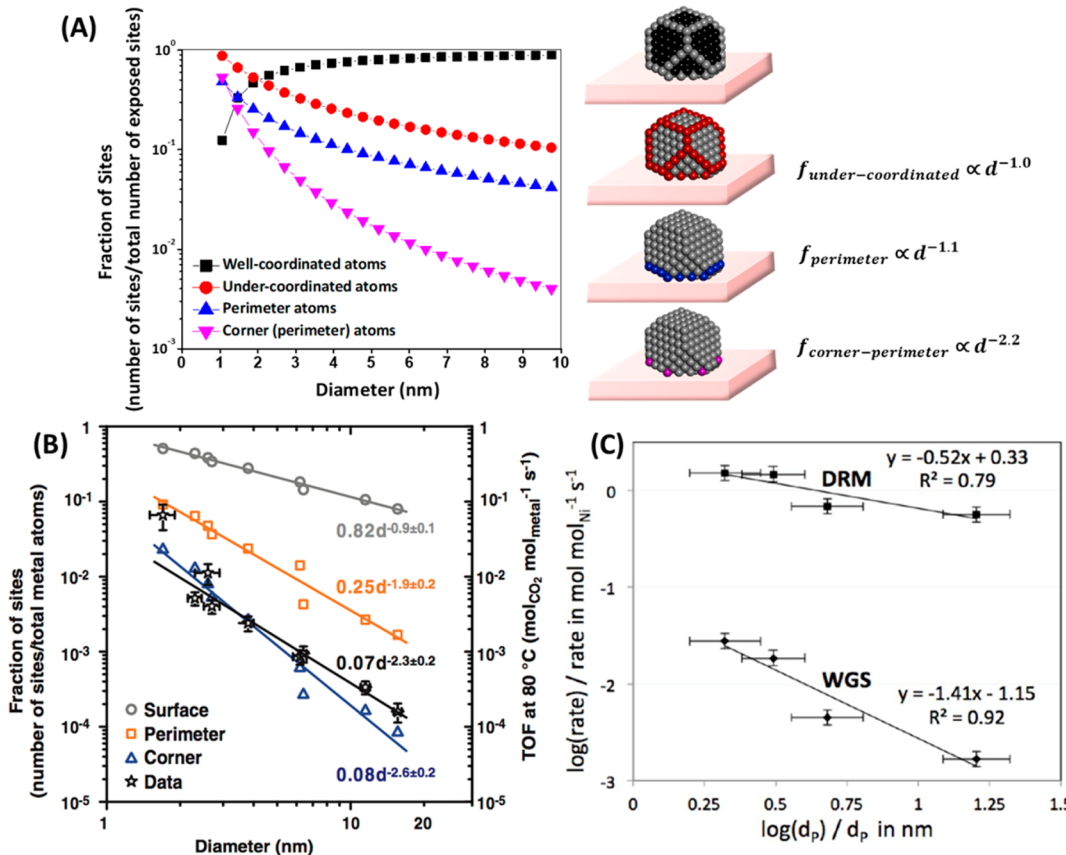


Figure 1. (A) Fraction (f) of various types of sites as a function of metal particle size calculated from geometric models. Adapted with permission from refs 44,45 Copyright 2014, 2016 American Chemical Society. (B) Calculated fraction of sites with a particular geometry (on total metal atom basis, rather than surface atom basis, as in (A)) and turnover frequency (TOF) on a total metal atom basis for CO oxidation on CeO_2 supported Ni, Pd, and Pt catalysts as a function of metal particle size. Reprinted with permission from ref 49. Copyright 2013 Science AAAS. (C) Reaction rate on the basis of total amount of Ni for water gas shift (WGS) at 300 °C and dry reforming of methane (DRM) at 650 °C on Ni/ Al_2O_3 catalysts as a function of Ni particle size. Reprinted with permission from ref 65. Copyright 2017 American Chemical Society. The differences in power law exponents in (A) and (B,C) stems from normalization by surface metal atoms and total metal atoms, respectively.

the reducibility of oxide supports.^{23–25} The metal-enhanced reducibility of oxide supports enables the direct participation of lattice oxygen in redox catalytic processes. Furthermore, the finding in the late 1970s that metal-promoted support reduction could initiate the encapsulation of supported metal particles, an effect called strong metal–support interactions (SMSI), was a spark igniting excitement in metal–support interactions.^{1,6–9} Finally, it has been demonstrated that sites at metal–support interfaces can enable bifunctional reactivity, opening unique mechanistic pathways for catalytic processes that cannot occur at metal sites alone.^{26,27} These various effects, which fall under the broad umbrella of metal–support interactions, have been summarized with specific instances described in previous reviews.^{6,7,28–31} The significance of these effects on the catalytic properties of supported metals is dependent on support composition and the relative amount of geometric interaction between the active metal and support, which is controlled by the ratio of the metal–support interfacial area to the exposed active metal surface area.

The goal of this Perspective is to highlight recent progress and analysis of approaches for maximizing metal–support interactions, and describe how maximized interactions influence the chemical and catalytic properties of supported metal active sites. Rather than focusing on the influence of oxide composition, we focus on approaches for geometrically maximizing metal–support interactions and the consequences

on chemical and catalytic properties.^{2,11,32,33} In this context, we start by describing how active metal species are modified by interactions with supports as they decrease in size from few nanometer diameter particles down to atomically dispersed species. We then describe an alternative approach to maximizing metal–support interactions through the in situ or ex situ overgrowth of oxides onto metallic structures. We pay particular attention to how microscopy, spectroscopy, and theory are correlated to provide insights. We end with a forward-looking discussion on the frontiers in this field and the potential for introducing unique catalytic behaviors by controlling the quantity and nature of metal–support interfaces, with the ultimate idea of creating catalytic architectures with homogeneous distributions of active sites that exist solely as active metal–support interfaces.

2. INFLUENCE OF ACTIVE METAL STRUCTURE SIZE ON METAL–OXIDE INTERFACES

In this section, we describe how changing the size of supported metal structures influences interactions between the metal and the support and in turn chemical and catalytic properties. We start by taking a simplistic view, where changing particle size is related solely to variations in the relative fraction of total exposed metal sites that exist at the metal–support interface. We then describe metal–support interfaces; specifically

focusing on how formation of this interface influences the charge of the interfacial metal sites (are they still metal?) and how the metal influences the reducibility of the support. This section is concluded with a perspective on important areas of research that will push the boundaries of this field forward, particularly understanding how properties of interfacial sites change as the catalytically active structure shrinks in size or dimension from a few nm diameter to atomically dispersed species—such as single atoms or atomically flat pancakes—where metallic character is lost.

2.1. Exposed Active Sites and Reactivity as a Function of Metal Particle Size. As the diameter of a supported metal particle shrinks from ~10 to ~1 nm, the relative fraction of exposed atoms existing in different local environments varies. Geometric models predict that the fraction of total exposed metal atoms that are under-coordinated (local metal coordination number <7) increases from ~0.15 to ~1 as metal particle size decreases from 10 to 1 nm, depending functionally on the inverse of particle diameter ($1/d$), Figure 1A. The fraction of different types of sites is influenced by the nanoparticle size, as well as shape. The shape of metal nanoparticles on a support is governed by the interfacial free energy between the metal and the support and the surface free energy, quantitatively described by the Winterbottom construction.^{34,35} This change in coordination environment of exposed metal atoms as a function of particle size and the resultant effect on reactivity has been extensively explored in the context of structure sensitivity.^{36–42} Variation in metal particle size over the same size range has a similar influence on the fraction of total metal atoms at the metal–support interface, where the fraction increases from ~0.03 to 0.3 as the size decreases from 10 to 1 nm, and again follows a $\sim(1/d)$ functional dependence on particle diameter, see Figure 1A.^{43–45} This means that differentiation of the influence of structure sensitivity and metal–support interfaces on catalytic behavior requires particle-size-dependent measurements across multiple supports that are expected to exhibit different influence on the catalytic reaction.

An excellent example of identifying the role of interfacial sites in catalytic processes by measuring particle-size-dependent catalytic performance is the case of CO oxidation ($\text{CO} + 1/2 \text{O}_2 \rightarrow \text{CO}_2$) over Pt group metals deposited on CeO_2 . It has been demonstrated that when Pt group metals are supported on irreducible oxides, such as Al_2O_3 , the CO oxidation turnover frequency (TOF, reaction rate per exposed active site) weakly depends on the metal particle size (in the range of ~1.5–20 nm diameter) when operating under conditions where the metal surface is saturated in CO.^{45–47} The minimal particle size dependence is due to a combination of the primary active site being well-coordinated Pt atoms and CO induced reconstruction of Pt surfaces.^{45,46,48} Alternatively, it was shown that for Pt, Pd and Ni on CeO_2 (in the range of 2–10 nm diameter) that the CO oxidation TOF depends on particle size with a $(1/d)^{1.3}$ functional dependence, see Figure 1B.⁴⁹ Under identical conditions when CO oxidation is executed on Al_2O_3 supported Pt-group metals the rate law is rate $\propto \frac{P_{\text{O}_2}}{P_{\text{CO}}}$, while on CeO_2 the rate law is rate $\propto P_{\text{O}_2}^{0.5}$, and further, the TOF is significantly enhanced on CeO_2 as compared to Al_2O_3 .^{49,50} The differences in TOF, rate law, and particle-size-dependence rates for CO oxidation on CeO_2 and Al_2O_3 oxide supported Pt-group metals are evidence that the reaction primarily occurs at metal–support interface sites

when reducible oxides are used as supports, whereas the reaction occurs on metallic sites when irreducible oxides are used as a support. This mechanistic difference stems from the involvement of lattice oxygen in reducible oxides in the catalytic cycle through a Mars–van Krevelen mechanism, which is not energetically feasible on irreducible oxides. Mechanistic conclusions regarding the importance of metal–support interface sites for lattice oxygen participation in oxidation catalysis on reducible oxide supported metals are consistent for CH_4 oxidation on similar systems and CO oxidation on Au catalysts.^{32,51–56} Rather than directly using metal particle size to relate interfacial site density to reactivity, spectroscopic signatures such as metal–O coordination number measured via X-ray Absorption Fine Structure (XAFS) have similarly been related to reactivity to implicate the role of interfacial sites for oxidation catalysis.^{57–62}

Another illustrative example of identifying interfacial atoms as active sites is the case of the water gas shift ($\text{CO} + \text{H}_2\text{O} \rightarrow \text{CO}_2 + \text{H}_2$, WGS) reaction on supported Au catalysts. Measurements of WGS TOF as a function of Au particle size (between ~1–5 nm diameter) for Au/TiO_2 catalysts showed the functional form $\text{TOF} \sim (1/d)^{1.7}$, which led to the conclusion that under-coordinated corner Au atoms (not those at the $\text{Au}-\text{TiO}_2$ interface) were the active site.⁶³ Further analysis showed that a similar dependence of WGS TOF was observed for $\text{Au}/\text{Al}_2\text{O}_3$ ($\text{TOF} \sim (1/d)^{1.2}$), although the rate was 20x higher for Au/TiO_2 as compared to $\text{Au}/\text{Al}_2\text{O}_3$.⁴⁴ Detailed kinetic studies, along with the magnitude of the support impact on TOF, suggested that for both catalysts the Au-support interface atoms are the active site, rather than corner atoms away from the support as proposed based on the analysis of only Au/TiO_2 catalysts.⁴⁴ This result is consistent with the observation of cationic Au species being the active site in WGS catalysis; the charge on interfacial metal atoms is discussed further below.⁶⁴ It was proposed that the metal–support interface facilitates H_2O activation and that differences in the barrier for H_2O activation at the interface were responsible for the rate dependence on the support.⁴⁴ This example highlights the importance of studying multiple supports when using particle-size-dependent measurements to identify the role of interfacial active sites and that interfaces between metals and irreducible oxide supports can also provide unique reactivity compared to the metal alone.⁴⁴

Recently, the role of interfacial sites was examined for $\text{Ni}/\text{Al}_2\text{O}_3$ catalysts in the WGS and dry reforming of methane ($\text{CO}_2 + \text{CH}_4 \rightarrow 2\text{CO} + 2\text{H}_2$, DRM) reactions, which mechanistically involve similar intermediates and elementary steps, but occur at different temperatures (300 °C for WGS and 650 °C for DRM).⁶⁵ It was observed that the rate depends more strongly on Ni particle size for WGS than for DRM (in the range of 2–16 nm diameter), Figure 1C. Through comparison to microkinetic models, it was elucidated that in both cases oxygenate species were involved in the rate-limiting step. Under WGS conditions, the Ni surface is poisoned by CO, thus OH species supplied by the support at the interface are required. Alternatively, under DRM conditions, the Ni surface is sufficiently clean, such that O and OH species are available on Ni and the interfacial supply of reactive oxygenates is not needed. This case highlights how adsorbate coverage can control the importance of metal–support interface sites. Similar effects in which the importance of the metal–support interface changes with feed conditions have been observed during CO oxidation, specifically that reactivity is insensitive to

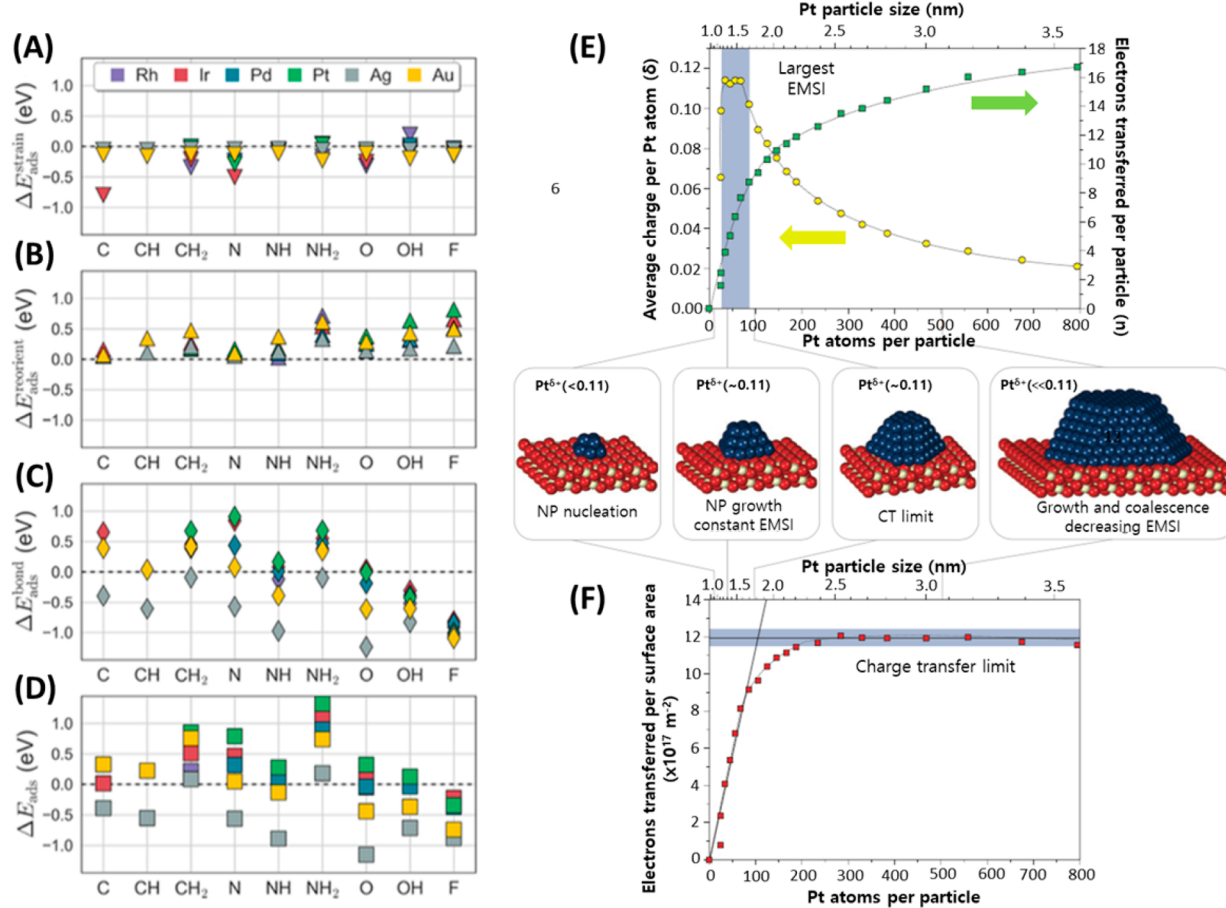


Figure 2. DFT calculated influence of (A) strain ($\Delta E_{\text{ads}}^{\text{strain}}$), (B) reorientation ($\Delta E_{\text{ads}}^{\text{reorient}}$) and (C) bonding effect ($\Delta E_{\text{ads}}^{\text{bond}}$) on the (D) change in adsorption energy (ΔE_{ads}) induced by the formation of metal-MgO bonds for a range of adsorbates. The different colored markers in each plot correlate to the results on different metals. Reprinted with permission from ref 77. Copyright 2017 American Chemical Society. (E) The measured number of electrons transferred per Pt particle (green) and resulting partial charge per Pt atom (yellow) as a function of Pt particle size (or number of Pt atoms per particle) measured for Pt/CeO₂ catalysts. (F) Electrons transferred per surface area (this is the Pt–CeO₂ interfacial area) as a function of Pt particle size. Schematics shown between (E) and (F) depict atomic models of the Pt particles and their charge in each size regime. Reprinted with permission from ref 21. Copyright 2015 Nature Publishing Group.

the support under low CO partial pressures or in the presence of water.^{50,66–71} This occurs due to the metal–support interface effectively being drowned out and emergence of the involvement of protons in the water layer facilitating the catalytic reaction at the metal–water interface.

These cases demonstrate how the roles of interfacial sites in catalytic cycles have been elucidated using metal particle-size-dependent measurements. The participation of interfacial oxygen in catalytic cycles on reducible oxide supported catalysts, activation of H₂O at interfacial sites and influence of adsorbate coverage on the importance of interfacial sites were each described. Other unique influences of interfacial sites on catalytic mechanisms certainly exist, with important implications on selectivity as well as activity.^{72–75}

With the role of interfacial sites implicated in many cases, it is important to ask, what makes interfacial sites unique? One potential explanation is that these are bifunctional sites that enable the interface to break down scaling relationships that would exist for the metal or oxide alone.^{76–78} It is noteworthy that bifunctionality only enables reactivity that is not confined by volcano behavior when two types of sites with largely different Brønsted–Evans–Polyani (BEP) and scaling relationships are coupled (i.e., metal and oxides sites, as compared to two different types of metal sites).^{79,80} However, in addition to

the bifunctionality imparted by the colocalization of metal and oxide sites, modification of the respective behavior of both the metal and the support due to the formation of bonds between them must be considered. It is possible that both metal and support sites at the interface possess unique properties compared to sites away from this interface, and this is what imparts unique catalytic properties on interfacial sites.

2.2. How Is the Metal Affected by Interface Formation? The influence of metal–oxide interface formation on the properties of the metal has been studied using density functional theory (DFT) calculations. By exploiting large unit cells that contain supported nanoparticles, or often nanowires, the influence of interface formation can be examined by calculating the adsorption or reaction energies on sites at the interface and away from the interface.⁷⁷ It has been reported for small Pt particles on TiO₂ that interfacial Pt atoms bind CO weaker (for example ~ by 1 eV) than Pt atoms sitting away from the interface.⁸¹ Alternatively for the case of Ni particles on Al₂O₃, it was found that interfacial Ni sites bind CO, CH₄, and CO₂ stronger than Ni sites away from the interface.⁶⁵ These reports, and various others examining supported Au catalysts, paint a picture that interfacial metal atoms exhibit different properties as compared to metal atoms

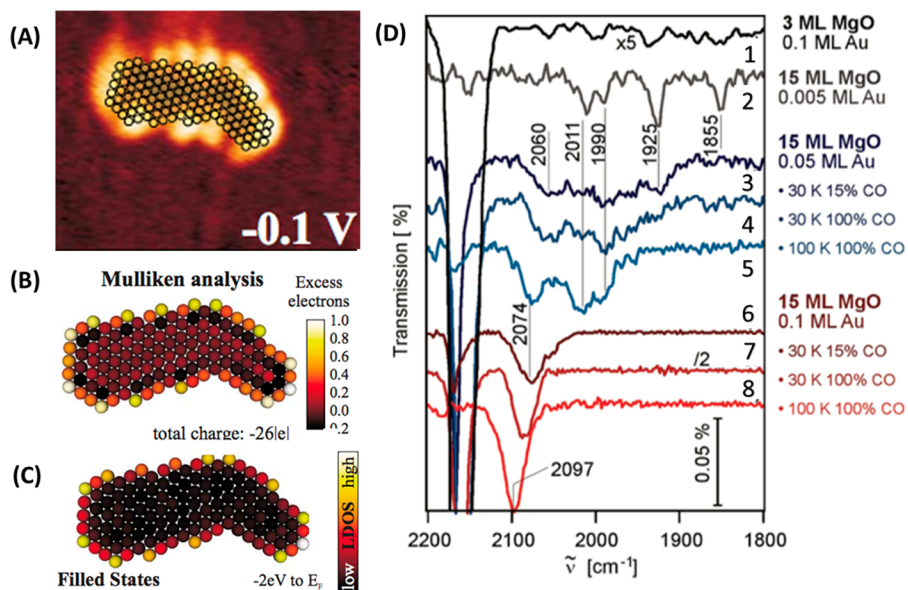


Figure 3. (A) Differential conductance (dI/dV) maps of an Au island on MgO at -0.1 V applied bias voltage. Overlayed on the image is the proposed structure of the Au island. (B) Calculated charge distribution of the Au island via Mulliken analysis. (C) The relative population of filled local density of states (LDOS) from 2 eV below the Fermi level to the Fermi Level (this is what is being probed experimentally in A). Reprinted with permission from ref 86. Copyright 2010 American Physical Society. (D) Infrared absorption spectrum of CO adsorbed on (1) a 3 ML MgO/ $\text{Ag}(001)$ film covered with 0.1 ML Au, (2–8) an electron-bombarded 15 ML thick MgO/Mo film covered with different Au coverages under different annealing temperatures and CO coverage. Reprinted with permission from ref 87. Copyright 2017 American Chemical Society.

away from the interface, although insights into the factors that dictate this behavior are complex.^{27,65,77,81–84}

Recently, a detailed computational analysis of the influence of interface formation between various metals and MgO was executed for a range of adsorbates.⁷⁷ This study also performed “control” calculations to ensure that the special behavior of interfacial metal atoms was not due to their low coordination numbers, but rather to their modified coordination environments. As depicted in Figure 2A–D, the analysis showed that the interface can induce both stronger and weaker bonding of adsorbates, ΔE_{ads} , as compared to metal sites away from the interface, and that the behavior can be understood in terms of 3 competing factors: (1) strain ($\Delta E_{\text{ads}}^{\text{strain}}$), or a change in metal–metal bond distances for interfacial metal atoms; (2) reorientation ($\Delta E_{\text{ads}}^{\text{reorient}}$), which causes the adsorbate to change binding geometry to the metal; and (3) bonding ($\Delta E_{\text{ads}}^{\text{bond}}$), where this effect encompasses changes in electronic structure of the metal atom and charge transfer to the adsorbate. In general, it was observed that modification of the inherent bond between the adsorbate and the metal induced by interface formation had the most significant influences on reactivity. This study clearly demonstrated that interfacial metal atoms are modified in their electronic structure and how they interact with adsorbates, and that the details of these interactions depend on the metal, adsorbate, and likely the support (although this was not explicitly examined in this study).

While DFT calculations can directly probe the influence of interface formation on the properties of interfacial atoms, experimental measurement of the influence of interface formation on the properties of metal atoms is challenging. However, important measurements have been made that shine light on the special properties of interfacial metal atoms. Particularly, charge transfer induced by interface formation, localization of charge to periphery metal atoms and the resulting influence of localization on adsorbate properties have been demonstrated for a select few cases.

It has been understood for some time that charge is exchanged between metal nanostructures and oxides upon interface formation.²⁸ However, quantitative measurement of the amount of charge transfer and the dependence on metal nanostructure size has proven challenging. This challenge arises because common techniques to make these measurements, such as photoelectron spectroscopy of the metal states, are influenced by a combination of initial state changes induced by charge transfer and final state effects that vary with metal particle size. To overcome this, a recent analysis of Pt/CeO₂ model catalysts used resonant photoemission spectroscopy to quantify the concentration of Ce⁴⁺ species that are converted into Ce³⁺ species in response to interface formation with Pt particles of sizes ranging from 10s to 100s of atoms ($\sim 1\text{--}4$ nm diameter).^{21,85} Using this approach, it was identified that the amount of charge transferred from Pt into CeO₂ per Pt atom increased from the smallest Pt particles to those in the size range of 30–70 atoms, and then declined above this size with a limit of 17% of Ce surface atoms (corresponding to 12×10^{17} m⁻² of electrons transferred per surface area) being reduced to Ce³⁺, see Figure 2E,F. This work provides direct evidence and quantification of charge transfer from Pt into CeO₂, rendering Pt cationic and stabilizing reduced Ce³⁺, and demonstrates that the amount of charge transfer per Pt atom is maximized at Pt particles in the size range of ~ 1 nm diameter. It is important to point out that in this case the influence of total Pt coverage on CeO₂ and Pt particle size on charge transfer could not be differentiated.

While experimental analysis of the Pt/CeO₂ system was able to quantify charge transfer induced by interface formation, the locale of the depleted charge of Pt was not identified—were electrons taken homogeneously from Pt or was this a localized effect? An analysis of planar Au islands on MgO by scanning tunneling microscopy and theoretical calculations demonstrated that interface formation induced electron transfer from MgO into Au. Charge flow in the opposite direction to the Pt-

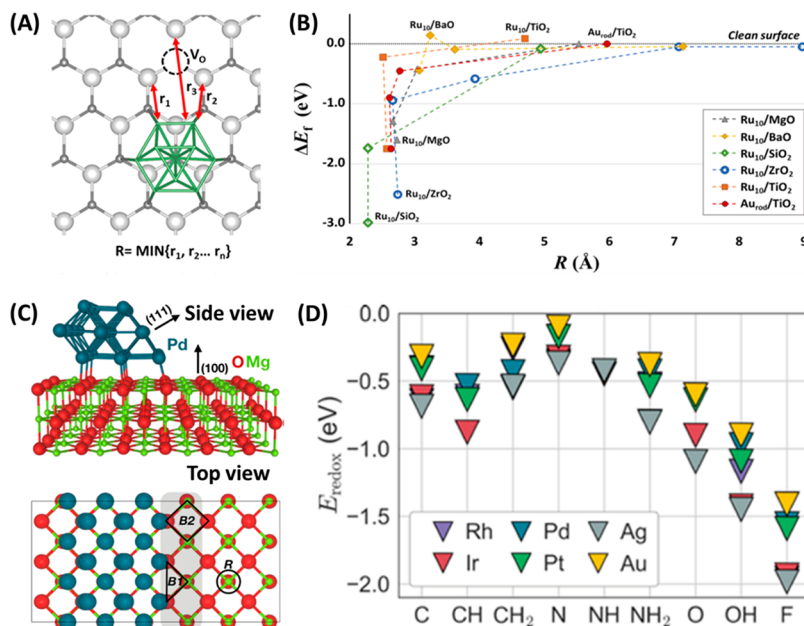


Figure 4. (A) Structural model defining the oxygen vacancy–metal cluster distance (R), where R is defined as the minimum distance between any supported metal atom and a cation surrounding the oxygen vacancy. (B) Change in the oxygen vacancy formation energy (ΔE_f eV) as a function of R for 10 atom Ru clusters on a few different supports and Au on TiO_2 . Reprinted with permission from ref 93. Copyright 2017 American Chemical Society. (C) Side and top views of a metal nanowire supported MgO (100), model systems. Proposed boundary adsorption sites are marked B1 and B2, and R refers an atop-Mg site remote from metal–oxide boundary. (D) Redox stabilization energy, E_{redox} for different adsorbates and metal compositions at site R . Reprinted with permission from ref 77. Copyright 2017 American Chemical Society.

CeO_2 system was due to the support consisting of thin oxide layers on metal films and the basicity of MgO . By spatially resolving the local density of states through differential conductance (dI/dV) measurements and comparing the results to theoretical calculations it was shown that transferred charge was localized at interfacial Au atoms and the amount of charge transfer per island was dictated by the filling of Au 6s states of interfacial atoms, Figure 3A–C.⁸⁶ In parallel to the Pt/CeO_2 case, charge localization at interfacial atoms was only observed when the island size was above ~ 50 Au atoms, where below this size limit molecular-like behavior existed for the Au islands in the sense that distinct lobe patterns could be observed across the whole island.⁸⁶ This analysis was extended to show that CO adsorbed to interfacial Au atoms have red-shifted vibrational frequency as compared to on the surface of larger Au particles, evidence of the negative charge state of the interfacial atoms, Figure 3D.^{87,88} The CO stretching frequency was blueshifted with increasing Au particle size after higher annealing temperature (100 K) and increased Au coverage from 0.005 to 0.1 ML.

It is apparent from this discussion that the formation of metal–oxide interfaces induces changes in the behavior of interfacial metal atoms. Most notably, the interfacial metal atoms exchange charge with the support, rendering them partially cationic or anionic, and these changes in charge state influence their catalytic properties. It is also clear that the specific differences in chemical and catalytic properties of metal atoms at the interface, compared to away from the interface, are a function of the metal, support, and adsorbate. This conclusion lends itself to the idea that the support and adsorbate act as ligands that modify the interfacial metal site electronic and physical structure, even in relatively large (i.e., not molecular) metal clusters.^{89,90}

In the context of understanding how the metal structure size influences interfacial metal properties, it is plausible that when structures are larger than 1 nm in diameter (in the “scalable regime”) that charge transfer primarily influences the properties of interfacial metal atoms and that these peripheral sites have similar properties regardless of metal structure size.^{85,91} Whereas below 1 nm diameter the “metal” structures lose their metal character and their interactions with the support and interfacial metal atoms may have inherently different properties than on larger particles. This will be discussed in more detail in Section 2.4.

2.3. How Is the Support Affected by Interface Formation? The formation of metal–support interfaces can also influence properties of the support. From the discussion of the Pt/CeO_2 system, it was shown that Pt donated charge to CeO_2 resulting in reduction of Ce^{4+} to Ce^{3+} , which certainly influences the chemical and catalytic properties of the CeO_2 surface.^{21,23,85} The most commonly discussed influence is the decrease in oxygen vacancy formation energy that occurs upon the deposition of metal particles and clusters.⁹² This was recently described in a Perspective and will only be briefly summarized here.⁹³ It is seen across a broad range of supports and metals that the addition of metals to an oxide support decreases the oxygen vacancy formation energy by up to a few eV, see Figure 4A,B.^{3,93} This effect is localized, primarily influencing the nearest neighbor oxygen to the metal cluster. The result is the stabilization of significant oxygen vacancy concentrations at the support surface under reducing environments that are not stable for the bare oxide.⁹⁴ Catalytically, this enables the involvement of lattice oxygen vacancies in the support in catalytic cycles through processes such as reverse oxygen spillover and Mars–van Krevelen reaction mechanisms.^{25,95–97}

Decreased oxygen vacancy formation energies at metal–oxide interfaces are consistent with the picture of electrons transferring from the metal to the support to promote the reduction process. Further evidence for this is provided by a recent theoretical analysis examining the influence of interface formation between various compositions of metal nanowires and MgO on the adsorption energy of molecular and atomic species on an Mg site two lattice spacings from the interface, Figure 4C,D.⁷⁷ It was observed that regardless of the metal and for a range of adsorbates that the addition of the metal to MgO increased adsorption energies by >0.5 eV. This effect was enhanced for adsorbates with higher electron affinities and generally for metals with low work functions. This suggests that the primary influence of metal–support interface formation on the reactivity of the oxide is through charge transfer between the metal and the oxide, which can promote reducibility and binding energies of adsorbates, thereby inducing unique catalytic functionality for oxide sites near the metal.

The influence of metal particle size on the promotion of oxygen vacancy formation is difficult to address, because differentiating particle size and total metal loading effects is challenging. At the limit of small metal clusters, theoretical calculations have found differing behavior for Au and Pt clusters. For Pt clusters including 3 or 8 atoms, the relative influence on TiO₂ reducibility was observed to be similar.^{81,98} Whereas for Au on TiO₂, it was identified that 10 atom Au clusters were significantly more effective for promoting vacancy formation compared to 3 atom clusters. Differences in these results should not be surprising as these clusters are no longer metallic and thus have unique size dependent properties. These analyses may also not tell a complete story, as clusters of this size exist in degenerate geometries that can exhibit different behavior. However, in the size range of >1 nm metal particles and at the limit of low coverage of the metal on the support, it has been suggested that the interfacial perimeter concentration controls vacancy formation, rather than any inherent metal particle size effects.²³

2.4. Interface Effects at Small (1–10 nm) and Very Small (<1 nm) Metal Clusters. From the discussion above, we can draw conclusions on how metal particle size influences the reactivity of interfacial sites and highlight areas of interest that are not completely understood. It is apparent that for certain catalysts and reactions, interfacial sites can be the predominant active sites. By shrinking metal particle size, the fraction of exposed sites existing as interfacial sites is enhanced, enabling tuning of reactivity and selectivity. In the size range of ~1–10 nm diameter metal particles, consistent trends in rate, apparent activation barriers, and reaction orders suggest that the interfacial sites are similar in physical, chemical, and catalytic properties and that metal particle size only plays the role of dictating the concentration of these sites. This makes sense as 1 nm particles contain ~50–100 atoms, have well-defined structures (physical and metallic electronic) and locally interfacial metal atoms have a similar coordination environment (up to the second nearest neighbor) on 1 nm particles as on 10 nm particles.

Much less is understood about trends in the reactivity of interfacial sites in the size range below 1 nm diameter. In this size range, clusters lose their metallic electronic structure, exhibit nonscaling behavior in their inherent reactivity (i.e., fluctuate in reactivity as a function of size)^{99–102} and can be dynamic in their structures.^{103–107} In contrast to metal

particles >1 nm diameter, in the smallest size range interfacial atoms have local coordination environments that vary as a function of cluster size. This is expected to influence the charge state, electronic structure, and rigidity of the interfacial sites, which are all expected to control catalytic performance.⁸⁹ It is expected that for the smallest limit of single atom active sites, where every site is an interfacial site, the local coordination environment will completely dictate the charge state of the atom, and that the chemical and catalytic properties of these active sites are more completely described by considering the atom and its surroundings, rather than just the single atom itself. Regardless of expected uniqueness in the <1 nm particle size regime, a few recent reports have suggested that the scaling relationships observed for particles >1 nm continue to hold their trend in the small size regimes.^{92,108} While a majority of the insights in the smallest size regime stem from “model catalysts”, the development of experimental approaches to probe the electronic structure and charge state of interfacial metal atoms on technical catalysts containing clusters with size <1 nm would be an important advancement in the understanding of the uniqueness of these sites.^{23,109} It is also interesting to consider if consistent trends in the reactivity of interfaces across broad ranges in metal particle sizes could be due to common dynamic behavior, for example, the recently proposed boomerang like emission of single atoms that can be uniquely reactive.^{110,111} From this discussion, it is apparent that obtaining more detailed insights into the structure and dynamics of these sites is crucial.

3. STRONG METAL–SUPPORT INTERACTIONS: IN SITU SUPPORT OXIDE OVERLAYER FORMATION ON METAL NANOPARTICLES

One of the original findings that drove research into metal–support interactions and the reactivity of interfacial sites was the observation that high-temperature H₂ treatment of some reducible oxide supported Pt-group catalysts resulted in a suppression of CO and H₂ chemisorption. Following extensive debate, it was identified that for Pt-group metals on TiO₂, Fe₂O₃, Nb₂O₅, and a few other oxide supports that high-temperature hydrogen treatment reduced the support through the formation of oxygen vacancies and induced encapsulation of the metal by the support.^{1,6–9} Although the SMSI acronym has been overused in literature, the original association was with this process of support encapsulation of metals that induces a decrease in chemisorption capacity of the metal. We caution that the term SMSI should not be used broadly as a “catch-all” for describing the many various interactions that occur between a metal and support, because it has a specific meaning. Metal–support interactions (MSI) is a better acronym for broadly encompassing the various physical and chemical effects that are induced by forming metal–support interfaces. Excitement surrounding the originally described SMSI behavior stemmed from the idea that this approach could be used to partially decorate metals with oxide islands; thereby creating a plethora of metal–support interface sites that may have unique behavior. This idea proved to be difficult to achieve. In this section, we highlight recent work that has deepened understanding of SMSI and identified routes to exploit this phenomenon for influencing catalysis and describe cases where the story is not yet complete.

SMSI behavior associated with support encapsulation of metals has been reported on many times and described in recent reviews.^{29,112,113} Here we briefly summarize the

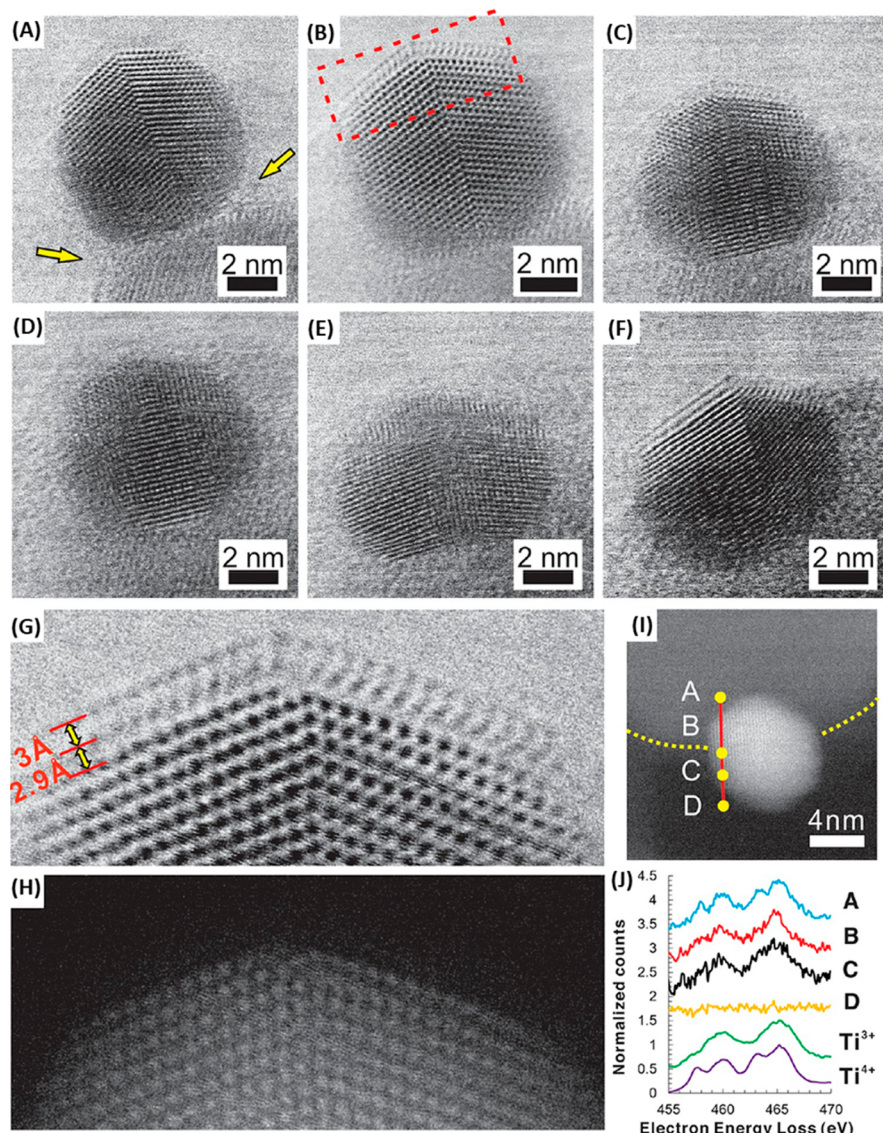


Figure 5. Representative sequential ABF images of an individual Pd nanocrystal supported on TiO₂ under reducing and oxidizing atmospheres. Pd/TiO₂ under reducing conditions (H₂ (5 vol %)/Ar at 1 atm) at (A) 250 °C, (B) 500 °C. Pd/TiO₂ under oxidizing conditions (150 Torr O₂) at (C) 250 °C for 8 min, (D) 250 °C for 15 min, (E) 500 °C. (F) Pd/TiO₂ under reducing conditions again (H₂ (5 vol %)/Ar at 1 atm) at 500 °C for 5 min. (G,H) Higher-magnification ABF and HAADF images, respectively, of a section of part (B) showing the TiO_x double layer. (I,J) EELS spectra extracted from a line scan of another particle under H₂ (5 vol %)/Ar at 1 atm and 500 °C with Ti³⁺ and Ti⁴⁺ reference spectra. Reprinted with permission from ref 114. Copyright 2016 American Chemical Society.¹¹⁴

understanding as reported in the most recent reviews and describe new findings, which have relied on the use of *in situ* transmission electron microscopy (TEM) at atmospheric pressure and elevated temperature.^{114–119} Developing insights into the SMSI state, particularly in the context of catalytic interfaces, can be grouped into three questions: 1. How much of the metal surface is coated by the oxide? 2. What structure does the overlayer have—amorphous, continuous, crystalline, porous? 3. Under what conditions is the overlayer stable?

The information to answer these questions has been derived from a combination of surface science studies on single crystals using scanning tunneling microscopy (STM) and ex situ analysis of high-surface-area supported metals via high resolution TEM. Taking the example of Pt, Pd, or Rh on TiO₂, both STM imaging on single crystals and TEM imaging of high surface area materials agree that upon reduction at ~500 °C, Pt is completely covered by TiO₂, which is

consistent with the original chemisorption analysis.^{120–127} However, differences have been observed regarding the structure of this overlayer. Surface science studies have shown crystalline TiO_x bilayers forming on Pt nanoparticles, whereas TEM analyses of high surface area materials have shown the existence of disordered or amorphous overlayers.^{122–127}

A recent attempt to address structural differences observed by STM and TEM was executed for the case of Pt on Fe₃O₄.¹²⁸ STM and TEM were used to examine materials consisting of Pt on single crystalline Fe₃O₄, and in both cases a single layer of FeO(111) was observed to form on the Pt surface in the SMSI state. However, significant differences were observed in the Pt–Fe bond distance at the metal–overlayer interface, which was attributed to oxidation of the FeO layer to form Pt–O–Fe–O observed in the TEM, rather than a Pt–Fe–O layer seen in the STM. These studies provide evidence that

differences in SMSI overlayers observed on single crystals via STM and TEM analysis of high-surface-area materials are likely derived from reoxidation of the overlayer that occurs during transport of the samples from the pretreatment reactors to the TEM.

Possible effects of postreduction exposure of the catalyst to air can be avoided by *in situ* TEM analysis. Advances in microelectromechanical systems technology allow for the execution of atomic resolution *in situ* TEM at elevated temperatures and in controlled gas composition at atmospheric pressure.¹²⁹ In a recent analysis of Pd nanoparticles on TiO₂, the formation of 3 unique overlayer structures was observed via *in situ* TEM during H₂ reduction, and the stability of these overlayer structures was examined.¹¹⁴ In an H₂ environment (5% at 1 atm) at 250 °C an amorphous layer of TiO_x was observed to form at the Pd-TiO₂ interface and on Pd away from the interface, Figure 5A. At 500 °C in H₂, the amorphous layer crystallized into a well-ordered bilayer of TiO_x, as shown in Figure 5B.¹¹⁴ Exposure to this bilayer to O₂, first at 250 °C (Figure 5C,D and further at 500 °C (Figure 5E) completely removed the TiO_x bilayer through filling of the oxygen vacancies creating a driving force to reform stoichiometric TiO₂ on the support surface, re-exposing Pd. 500 °C treatment in H₂ was shown to regrow the bilayer, Figure 5F, in excellent agreement with the known reversibility of the CO/H₂ chemisorption capacity when cycling through oxidation and reduction treatment.^{9,130} Detailed structural analysis via higher magnification annular bright field (ABF) and high-angle annular dark-field (HAADF), Figure 5G,H, and chemical analysis via *in situ* electron energy loss spectroscopy (EELS), Figure 5I,J, showed that the crystalline TiO_x overlayer clearly is a bilayer and predominantly contains Ti in a 3+ charge state. These results provide the first evidence of crystalline TiO_x SMSI on Pt-group metals from measurements on high surface area supported catalysts, give evidence of the chemical state of Ti in these layers, and solidifies the importance of *in situ* observation in understanding SMSI phenomena.

Guided by previous surface science studies, DFT calculations were used to examine the energetics of forming different structures and thicknesses of TiO_x layers on Pd, as shown in Figure 6. It was observed that as a function of decreasing oxygen chemical potential (stronger reducing environments), the most stable system would transform from a bare Pd surface (Figure 6D), to one layer of kagomé-structured TiO_{1.5} (Figure 6C) and then two layers of TiO_{1.5} (Figure 6B). On the basis of these studies, *in situ* TEM analysis at controlled reduction conditions was also able to identify a monolayer TiO_x crystalline structure. The Ti₂O₃ stoichiometry of the proposed layers is in good agreement with the *in situ* EELS measurements of predominantly Ti³⁺ in the overlayer.

The *in situ* TEM analysis was conclusive in demonstrating that SMSI overlayers observed via *ex situ* and *in situ* measurements identify different structures. The structures proposed based on the *in situ* TEM and DFT studies agree with combined surface science and DFT studies, providing convincing evidence of the overlayer structures.¹²⁰ It is clear that following high-temperature reduction of Pt-group metals on TiO₂, a crystalline and complete overlayer forms on the metal. The TEM and DFT studies also show that these crystalline overlayers are highly unstable with even slight increases in oxygen chemical potential, which could be provided by exposure to air or H₂O during catalytic process if water is a reactant or product. This allows rationalization of

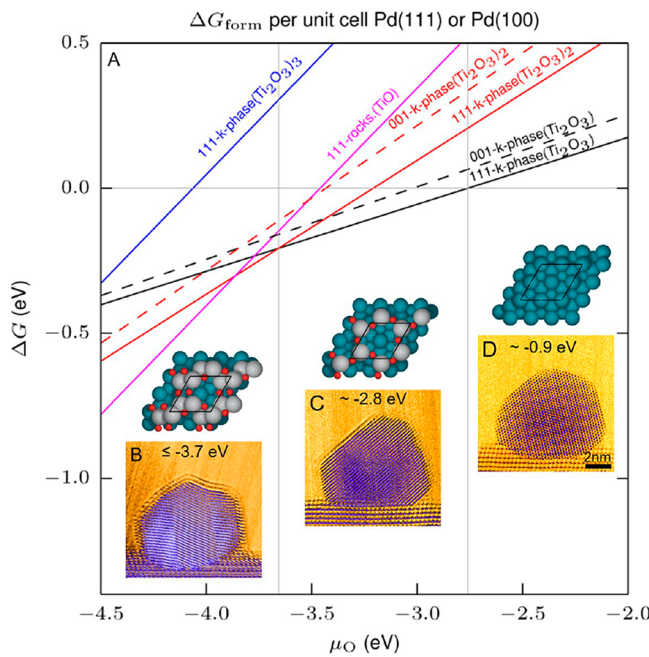


Figure 6. Computational and experimental characterization of TiO_x overlayers under different experimental conditions. (A) Theoretical calculations of free energy G for different TiO_x phases on Pd(111) or Pd(100) surfaces as a function of oxygen chemical potential (μ_O). (B) TiO_x double layer formation under H₂ (5 vol %)/Ar. (C) TiO_x single layer formation under H₂ (4.9 vol %)/O₂ (2 vol %)/Ar, (D) No layer formation under H₂ (4.7 vol %)/O₂ (5.7 vol %)/Ar. The top-down views of the corresponding structures of the experimentally observed surface layers are shown above the TEM images collected at 1 atm total pressure and 500 °C. Correspondence of colors and elements: Dark green, Pd; gray, Ti; red, O. Reprinted with permission from ref 114. Copyright 2016 American Chemical Society.

previous observations relating catalytic properties to SMSI behavior.

For the case of structure sensitive reactions, such as ethane hydrogenolysis, and in which no oxidizing reactants or products are present, the overlayer completely poisons the catalyst resulting in very little to no reactivity.^{131,132} For the case of structure-insensitive reactions that have low reaction barriers, such as cyclohexane dehydrogenation, where no oxidizing reactants or products are present, catalytic reactivity can still exist as the surface of thin oxide layers on metals are known to have distinct properties compared to the oxide itself.^{132–134} Similarly, for relatively low barrier reactions where selectivity is important, stable full encapsulation layers can influence reactivity, for example in crotonaldehyde hydrogenation (competing hydrogenation of C=C bond to butyraldehyde vs C=O bond to crotyl alcohol), where the SMSI overlayer enhances selectivity toward crotyl alcohol by coordinating crotonaldehyde through C=O bond.^{135,136} Finally, for the case of reactions where oxidizing agents are present, it is likely that the reduced overlayer is reoxidized and recedes off the metal, as shown in Figures 5 and 6, resulting in minimal impact on reactivity. While differences in behaviors certainly exist for other oxides (and *in situ* analysis is needed), it is clear that SMSI overlayers formed via high-temperature H₂ reduction do not form stable structures consisting of partial decoration of metal nanoparticles by oxide islands, which would produce high concentrations of interfacial sites. Thus,

the engineering of catalytic properties using SMSI overlayers to form interfacial sites has proven to be challenging.

Recently, an analysis of Rh/TiO₂ catalysts showed that treatment at 250 °C in 20% CO₂, 2% H₂ at 1 atm could induce the formation of an amorphous overlayer that was stable under conditions where H₂O was present and allowed for tuning of CO₂ hydrogenation selectivity.¹¹⁵ In situ scanning transmission electron microscopy (STEM) and EELS analysis demonstrated that whereas 550 °C treatment in H₂ produced the crystalline TiO_x bilayer seen previously for Pd/TiO₂, the CO₂/H₂ treatment produced a thin amorphous overlayer containing a mixture of Ti³⁺ and Ti⁴⁺, as shown in Figure 7A,B. The stability

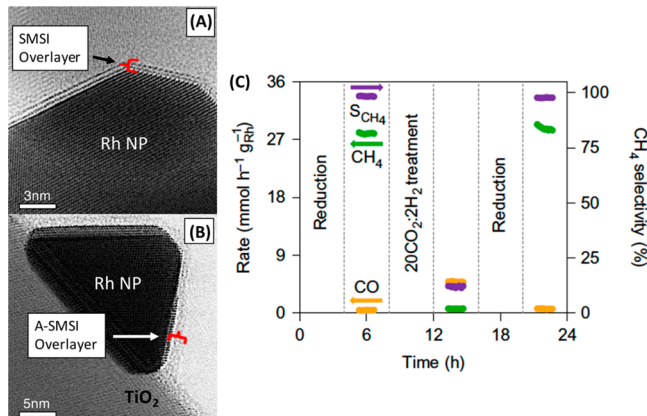


Figure 7. In situ TEM images of 6% Rh/TiO₂ showing the formation of (A) a TiO_x SMSI crystalline bilayer on the surface of Rh nanoparticles (NPs) after treatment in 5% H₂ and 95% N₂ at 550 °C for 10 min, and (B) an amorphous A-SMSI overlayer after treatment in 20% CO₂, 2% H₂ and 78% He at 250 °C for 3 h. (C) CO and CH₄ production rate and selectivity to CH₄ over 6% Rh/TiO₂ at 200 °C. Feed composition: 1% CO₂, 1% H₂ and 98% He, after pure H₂ treatments (denoted as reduction) at 450 °C for 4 h and then 20CO₂:2H₂ at 250 °C for 4 h. Reprinted with permission from ref 115. Copyright 2017 Nature Publishing Group.

of the amorphous layer in the presence of H₂O and existence of significant Ti⁴⁺ in the overlayer, suggested that this is not a typical SMSI layer. Through various analyses by in situ IR and comparison to previous work on single crystals, it was proposed that HCO_x species on the support drove oxygen vacancy formation that instigated the movement of TiO_x (likely functionalized with HCO_x) onto Rh. The HCO_x mediated overlayer formation was termed adsorbate-induced SMSI (A-SMSI), and it was further proposed that HCO_x coordination to TiO_x in the overlayer stabilized the overlayer against oxidation by H₂O. The stability of the A-SMSI overlayer in humid environments allowed comparison of the reactivity of the bare and A-SMSI overlayer covered Rh surfaces in CO₂ hydrogenation. It was observed that bare Rh is 100% selective for CH₄ production, as has been shown before, whereas in the A-SMSI state, the catalyst was 90% selective for CO formation, Figure 7C. This provides an example where an overlayer produced in response to support reduction resulted in a structure where essentially all exposed sites were interfacial sites that had distinct reactivity compared to the metal or oxide alone. Further, this highlights again the importance of in situ microscopy for understanding SMSI behavior.

With an understanding that the traditional SMSI overlayers only rarely find useful impact on catalytic performance, and further that overlayers can be produced and stabilized in humid

environments with the involvement of adsorbates on the support, it is interesting to consider how A-SMSI like behavior may play a role in controlling the performance of Cu/ZnO/Al₂O₃ methanol synthesis catalysts. Although this system has been intensely studied with the goal of identifying the active site, a detailed description has remained elusive. It is clear that undercoordinated Cu is necessary, that the ZnO-Cu interface promotes reactivity (either through Cu-Zn alloy formation or an interfacial effect), and that ZnO is quite dynamic on Cu surfaces forming various versions of SMSI overlayers.^{116,137–140} For example, a metastable disordered graphitic-like ZnO_x layer was observed on Cu particles via ex situ TEM following reduction at 250 °C for 90 min, as shown in Figure 8.¹¹⁶ It is

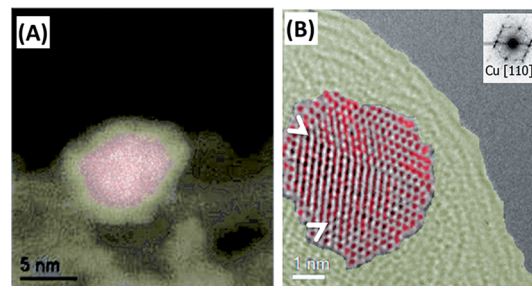


Figure 8. (A) Ex situ HAADF-STEM and (B) high-resolution transmission electron microscopy (HRTEM) images of a reduced Cu/ZnO/Al₂O₃ catalyst at different magnifications and areas. The images are false colored to identify Cu as pink/red and Zn in yellow/gold. The inset in (B) denotes a power spectrum, which allows identification of the Cu nanoparticle. The arrows in (B) mark twin boundaries. Reprinted with permission from ref 116. Copyright 2015 Wiley-VCH Verlag GmbH & Co. KGaA.

interesting to consider if the apparently unique and difficult to resolve active site properties Cu/ZnO/Al₂O₃ for methanol synthesis may be related to a flavor of ZnO SMSI overlayer that is stabilized against reoxidation by adsorbates. This is plausible as the conditions for methanol synthesis are not so different from those used in analysis of A-SMSI in the Rh/TiO₂ catalyst. Future in situ TEM analyses of the Cu/ZnO/Al₂O₃ catalyst are likely to help resolve this question.

We would like to add an important point in the context of in situ analysis. In situ TEM characterization is powerful to characterize morphology, crystal structure, defects, strain, and chemical information at atomic level. However, it should be noted that high-energy electron beam irradiations during analysis induces structural modifications of catalysts as reported previously.^{141–143} Therefore, care should be taken to ensure electron beam effects are minimized and information gained from TEM should be correlated to complementary information from other sample averaged characterization tools, such as infrared and X-ray absorption spectroscopy, to ensure that observed effects are not related solely to beam induced structural changes.¹⁴⁴

4. EX SITU DEPOSITION OF OXIDE OVERLAYS ON METAL NANOPARTICLES

With an understanding of the difficulties in controlling the structure of metal oxide overlayers formed on the surface of metal particles by in situ treatments, there has been significant interest in the intentional and controlled deposition of stable, porous oxide overlayers onto metals to produce metal-interface sites. Early studies aimed at investigating metal–oxide

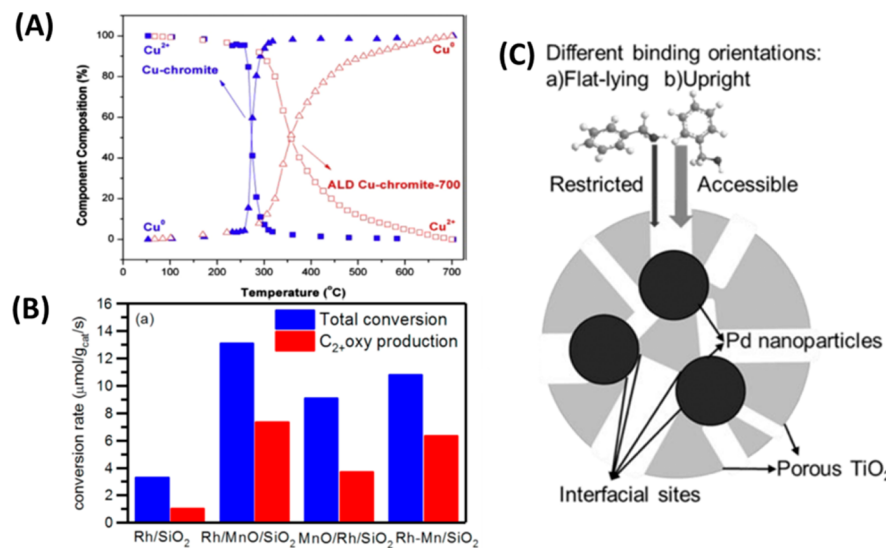


Figure 9. (A) In situ XANES spectra showing evolution of Cu species as a function of temperature for the Cu-chromite and ALD Cu-chromite catalysts. Reprinted with permission from ref 170. Copyright 2014 Elsevier. (B) Total CO conversion and C₂₊ oxy production. Rh–Mn/SiO₂: coimpregnated catalyst prepared for comparison. Reprinted with permission from ref 171. Copyright 2017 American Chemical Society. (C) Controlled binding as well as interfacial sites induced by nanoporous TiO₂ film. Reprinted with permission from ref 22. Copyright 2017 Wiley-VCH Verlag GmbH & Co. KGaA.

interfaces made use of model catalysts based on well-defined single metal crystals and vacuum deposition techniques.^{145–151} Both metal deposition on oxide substrates and inverse oxide/metal catalysts have been extensively studied and provide insights into the role of the oxide and the oxide–metal interface for a variety of catalytic reactions.^{148–151} Recent studies on well-defined inverse model catalysts have provided new insights into the consequences of structural, electronic, chemical, and catalytic properties at metal/oxide interfaces.^{152–162}

In contrast to model catalysts, the synthesis of high-surface-area catalysts with homogeneous and well-defined interfacial active sites through the intentional overcoating of oxide films on metal nanoparticles remains challenging. Below we describe recently developed synthetic protocols for forming controlled amounts of metal–oxide interfaces on high surface area catalysts. The initial application of these techniques focused mostly on stabilizing metals against sintering. However, these approaches have also found application in modifying catalysts' intrinsic activity and as a platform for understanding the properties of catalytic metal–support interfaces.

4.1. Atomic Layer Deposition (ALD) for Depositing Oxide Overlays.

Atomic layer deposition (ALD) is a vapor-phase technique that is attractive for forming interfaces with atomic-level precision. ALD uses sequential self-limiting surface reactions to allow uniform and conformal deposition of materials with atomic-scale control.¹⁶³ ALD was originally developed for thin film electroluminescent flat-panel displays in the 1960 and 1970s, but the application of ALD has been expanded to a wide range of industrial and research processes including photovoltaics, energy storage, and sensors because of its excellent film conformity, atomic level thickness control, and tunable film composition.^{163,164} ALD-based production of porous oxide films on metal nanoparticles was initially applied to improve catalyst thermal stability, by minimizing metal mobility, and prevent deactivation caused by coking and sintering.^{165–169} However, further interest in the use of ALD for catalytic applications came from observations that these

overlays can not only improve stability but also enhance reactivity and selectivity. Recent studies have demonstrated the utility of ALD oxide overlays for modifying the selectivity of metal catalysts, showing that Al₂O₃ overcoatings increased the ethylene yield of Pd catalysts by more than a factor of 10 in the oxidative dehydrogenation of ethane.¹⁶⁵ The Al₂O₃ ALD layer preferentially deposits on low-coordinated Pd surface sites, where C–C bond scission occurs, resulting in coke formation, while allowing ethylene formation to continue unperturbed on well-coordinated terrace sites.¹⁶⁵ In this case, the overlay primarily played the role of site blocking, rather than introducing unique reactivity at the metal–oxide interface.

Changes in catalytic activity as a result of metal oxide overlays deposited by ALD have also been demonstrated due to changes in oxidation state of the metal.¹⁷⁰ An example of such behavior is seen in Figure 9A, where it was observed that ALD of Al₂O₃ on Cu-chromite catalysts significantly modified the activation energy for reducing Cu²⁺ to Cu¹⁺ and Cu⁰, which in turn promoted the catalytic properties for furfural hydrogenation.¹⁷⁰ This shows directly that ALD can be used to form oxide–metal interfaces that introduce unique chemical and catalytic functionality at the interface. This result agrees quite well with interfacial effects discussed in the previous sections, suggesting that interfaces formed between metals and intentionally deposited oxide overlays are analogous to those formed between the metal and underlying support. However, it is worth noting that the similarity between thin oxide layers on metals and metal particles on bulk oxides is only highlighted here in terms of similarity in their influence on the metal oxidation state. The very different electronic structure between bulk and thin oxide layers is likely to drive significant differences in the chemical and catalytic properties of interfaces formed in these two geometries.

While the ALD approaches described above result in the deposition of oxide overlays both on the metal and original oxide support, a modified ALD overcoating approach using O₂ gas as coreactant was recently proposed that enabled the selective deposition of metal oxides on noble metal nano-

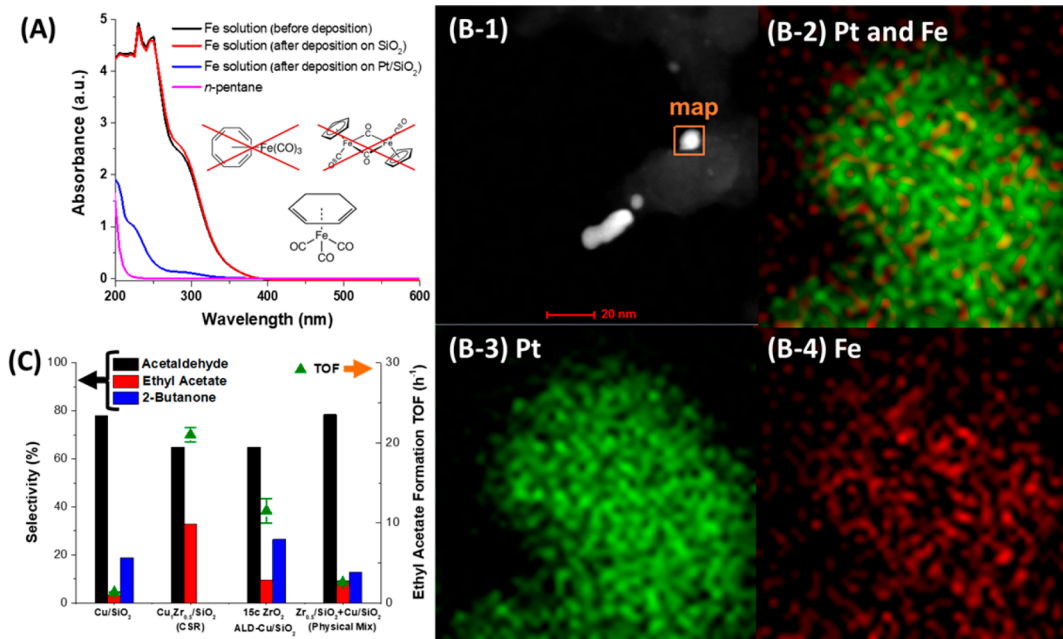


Figure 10. (A) UV–vis absorption spectra of Fe precursor ((cyclohexadiene)iron tricarbonyl) solution in *n*-pentane before (black) and after deposition onto the SiO₂ support (red) and Pt/SiO₂ (blue). Reproduced with permission from ref 183. Copyright 2016 American Chemical Society. (B) EDS mapping of Pt and Fe in Pt₁Fe_{0.2}/SiO₂ (a Fe/Pt molar ratio of 0.2). Correspondence of colors and elements: green, Pt; red, Fe. Unpublished work from ref 191. (C) Product distribution over Cu/SiO₂, Cu₁Zr_{0.5}/SiO₂ (CSR, a Zr/Cu molar ratio of 0.5), 15c ZrO₂–Cu/SiO₂ (15 ALD cycles of ZrO₂), and a physical mixture of Zr_{0.5}/SiO₂ and Cu/SiO₂ for the selective conversion of ethanol to ethyl acetate. Reproduced with permission from ref 183. Copyright 2016 American Chemical Society.

particles.^{171,172} MnO-modified Rh catalysts were prepared using the selective ALD technique by depositing MnO as a support layer under Rh (Rh/MnO/SiO₂) or an overlayer (MnO/Rh/SiO₂) on top of Rh and the catalytic performance in syngas conversion was evaluated.¹⁷¹ As shown in Figure 9B, the addition of MnO to Rh via either ALD (Rh/MnO/SiO₂ and MnO/Rh/SiO₂) or coimpregnation (Rh–Mn/SiO₂) increases conversion and selectivity to C₂₊ oxygenates. Interestingly, Rh/MnO/SiO₂ is more active and selective than MnO/Rh/SiO₂, and this was ascribed to the poor stability of MnO overlayers on Rh upon CO adsorption.¹⁷¹ This result is reminiscent of discussions above associated with SMSI behavior, where overcoatings of partially reduced oxide layers on metals can be unstable (i.e., recede off the metal) under reaction conditions. Thus, while the idea of selectively depositing the oxide overlayer on the metal through ALD, rather than on both the metal and support, is appealing, this seems to reduce the stability of the overlayer and the potential impact of metal–oxide interfaces on catalytic properties.

4.2. Wet Chemical Synthesis Approaches Depositing Oxide Overlayers. There are also a number of solution-based approaches for either depositing oxide overlayers on supported metal particles, or encapsulating colloidal metal particles with porous oxides that facilitate detailed analysis of interfacial effects. One approach that grew out of the massive amount of work in the 2000s in the field of colloidal synthesis of metal nanoparticles, is the hydrolysis of oxide precursors at the surface of ligand capped metal nanoparticles. In this approach, hydrolysis forms shells on the metal nanoparticle core that crystallize into oxide shells when heated in air. The use of ligands on the metal nanoparticles allows for the formation of pores once the ligands burn away during the oxide shell crystallization. This approach has been widely employed to increase the stability by protecting catalytically active core

nanostructures from deformation or aggregation, similar to ALD.^{173–177}

In addition to promoting metal stability, the porosity in oxide encapsulation layers synthesized through colloidal approaches has been regulated with the objective of controlling reactant binding geometries at the metal–oxide interface. In one such example, core–shell structures consisting of Pd nanoparticles and porous TiO₂ shells were synthesized and used in alcohol hydrodeoxygenation chemistry.²² The observed selectivity was consistent with the aromatic alcohols being restricted in their adsorption geometry on Pd to standing up, rather than lying down where direct ring–Pd interactions occurred. It was proposed that the enhanced reactivity and selectivity were due to a combination of the large concentration of Pd-TiO₂ interfacial sites exposed and the pore induced control of adsorption geometry, Figure 9C. These results demonstrate, similarly to the ALD discussion above, that controlled deposition of porous oxide layers on metals can enable tuning of reactivity through the introduction of a wealth of interfacial sites. The ability of porous oxide encapsulation layers to discriminate binding of certain intermediates relative to others parallels the effect of the confining voids of zeolitic materials.¹⁷⁸ The structure of these porous oxide coated particles could be similar to ALD-overcoated or to nanocavities generated using surface-grafted template molecules.^{165,179,180} Further studies of similar structures will likely provide deeper insight into whether formed interfacial sites are the primary cause of observed reactivity, or whether this is due to pore structures controlling the geometry of adsorbing species at exposed metal sites.

Another synthetic protocol aimed at producing materials with well-defined concentrations of interfacial sites is controlled surface reactions (CSR).^{181–190} CSR allows selective deposition of a promoting material on metal with

negligible deposition on the support.^{181,182,191} For example, UV-vis absorption spectra of a Fe compound ((cyclohexadiene)iron tricarbonyl) in *n*-pentane before and after contacting SiO₂ and Pt/SiO₂ is shown in Figure 10 A. Negligible uptake by pure SiO₂ but significant deposition on Pt/SiO₂ was observed, suggesting selective deposition of the Fe precursor on Pt sites. EDS mapping showing Fe domains collocated with Pt supports this assertion, Figure 10B.¹⁹¹ In contrast, experiments using (cyclooctatetraene)iron tricarbonyl and cyclopentadienyliron dicarbonyl dimer as Fe precursors led to nonselective deposition on both Pt sites and the SiO₂ support.¹⁸⁸ This suggests that the geometry and degree of unsaturation of the precursor complex are important for the selective deposition on metal sites, as shown in Figure 10 A.¹⁸⁸ Once Fe is deposited on Pt, it is expected that oxidation would result in the formation of Pt-FeO_x interfacial sites similar to the selective ALD case described above.

A comparison of interfacial sites produced via ALD and CSR was executed in the context of selective conversion of ethanol to ethyl acetate over Cu/SiO₂ catalysts to which ZrO₂ was added, Figure 10C.¹⁸³ A physical mixture of ZrO₂/SiO₂ and Cu/SiO₂ exhibited only a slight improvement in the rate of ethyl acetate formation and selectivity compared to Cu/SiO₂, suggesting that Cu-ZrO₂ interfacial sites are important for ethyl acetate production.¹⁸³ The addition of ZrO₂ (Cu₁Zr_{0.5}/SiO₂, a Zr/Cu molar ratio of 0.5) to Cu/SiO₂ via the CSR method increased the rate of ethyl acetate formation and suppressed the formation of the byproduct 2-butanone.¹⁸³ In contrast, deposition of ZrO₂ by ALD did not suppress butanone production, as dispersed ZrO₂ species on the SiO₂ support catalyzed the acetaldehyde condensation reaction.¹⁸³ The above example shows the benefit of the selectivity in deposition afforded by CSR compared to ALD, although the recent improvements in site selective ALD will allow a better comparison of how different approaches compare in their ability to produce targeted interfacial sites.

A final approach we highlight for the synthesis of supported metal catalysts with controlled interfacial sites is selective metal deposition onto targeted oxide domains via strong electrostatic adsorption (SEA). Interactions between terminal hydroxyl groups on metal oxide surfaces and charged metal precursors in solution can be tuned by adjusting the pH of the impregnating solution, which manipulates the charge on the metal oxide surface through protonation or deprotonation.^{192,193} At pH's below the point of zero charge (PZC) of the oxide, hydroxyl groups on metal oxide surfaces become protonated and thus positively charged, and interact with anionic metal complexes such as hexachloroplatinate complexes, [PtCl₆]²⁻.^{192,193} Above the PZC, hydroxyl groups on the metal oxide surface deprotonate and become negatively charged, and interact with cationic metal complexes such as platinum tetraammine complexes, [(NH₃)₄Pt]²⁺.^{192,193} This approach, combined with the understanding that different oxides have different PZC's, allows for the selective deposition of metals onto targeted oxides.^{193,194} For example, using the difference in the PZC values of silica (4.25) and alumina (8.0) and working at pH values between 6 and 8, a cationic precursor complex such as [(NH₃)₄Pt]²⁺ can be selectively deposited on the negatively charged silica surface, as illustrated in Figure 11. Using this approach, the activity of a series of metal-acid bifunctional catalysts with metal:acid ratios and metal-acid site proximity controlled via SEA was evaluated for *n*-heptane isomerization, where it was observed that control

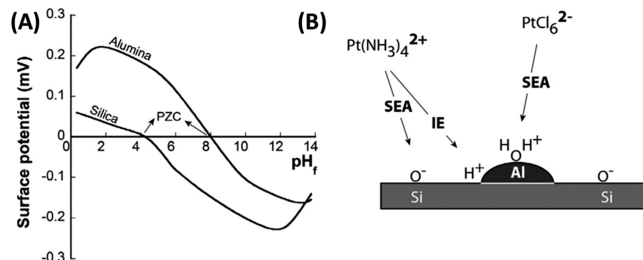


Figure 11. (A) Plot of theoretical surface potential versus pH for silica (PZC = 4.25) and alumina (PZC = 8.0). (B) Schematic illustration of surface charge of silica-alumina mixed oxide surface at intermediate pH (pH = 6–8) and interaction with Pt cationic/anionic metal complexes. Reprinted with permission from ref 194. Copyright 2016 Elsevier.

over where Pt deposited on aluminosilicate promoted the formation of interfacial metal-acid sites that enhanced catalytic properties.¹⁹⁵

5. CONCLUSIONS AND OUTLOOK

There has been a great deal of progress in understanding metal-support interactions after the onset of research in this area in the late 1970s. Metal-support interactions have been particularly extensively studied in the context of active sites at the interface of metal particles and oxide supports, and in cases where interfacial sites form due to oxide encapsulation layers on the metal surface, either as a result of pretreatments conditions or controlled oxide deposition. It is abundantly clear that in many catalytic processes the ability to engineer interfacial site composition, structure, and prevalence enables optimization of catalytic performance. However, much remains to be understood about the chemical and catalytic properties of active sites at the interface between metals and supports.

The first outstanding challenge is elucidating the behavior of interfacial sites for metal clusters in the size range of 1 nm diameter to the limit of single atoms. In this size range, the electronic and physical structure of supported metals are dynamic and interfacial sites are likely to exhibit unique local coordination, as compared with on larger metal particles and thus reactivity. However, it could also turn out that the ensemble average behavior of interfacial sites on metal clusters of this size follow trends observed for larger particles. In this case, clusters in the very small size range would allow for maximization of the prevalence of metal-support interface sites.

Another challenge is disentangling contributions of electronic effects introduced by the formation of a metal-support interface from the bifunctionality of two proximal types of sites that obey different scaling relations. It is likely that the relative importance of these two effects on catalytic activity will depend on the nature of the kinetically relevant steps in the reaction and the environmental conditions under which the reaction is conducted and further that both mechanisms play some role in any given system.

Finally, it is interesting to consider whether there exists an equivalence in behavior for interfaces formed by different geometries (i.e., a metal particle and support interface versus a porous encapsulation layer and underlying metal interface). In line with this question, the importance of the synthetic method used in forming interfacial sites and the resulting chemical and catalytic properties is currently ambiguous. In one interesting

example, it was observed that for both interfaces formed between single Rh atoms and a TiO₂ support and for A-SMSI porous overlayers of TiO_x on Rh particles CO₂ is selectively reduced to CO by H₂, whereas on bare Rh surfaces CH₄ is formed. Is this suggesting the interfaces between Rh and TiO₂ in very different structures have similar properties? Or is the situation more complex?^{115,196}

With advances in capabilities for synthesizing catalysts consisting of atomic-scale supported metal species and porous oxide overcoating layers with tunable properties, it seems that synthesis of catalysts with homogeneous distributions of well-defined interfacial sites is possible and will be achieved through a convergence of the discussed approaches.

It is also important to consider alternative analysis approaches to those described here in order to learn more about interfacial site properties. For example, kinetic studies using carefully chosen probe molecules are useful, as they provide a signal that is a direct consequence of the catalysis itself. Extensive work has been done using isotopically labeled or structurally modified reactants as probes.^{69,70,197–202} Recent work also applied Hammett studies to understand reactivity of the Au-catalyzed oxidation of benzyl alcohol. Hammett studies are performed by substituting the para position of a phenyl ring with groups of varying electron withdrawing capacity and measuring the effect of this substitution on the reaction rate.²⁰³ It has been shown that benzyl alcohol oxidation rates correlate linearly with the electron-withdrawing capacity of these substituents as these stabilize the positive charge on the benzylic carbon in the transition state of the kinetically relevant hydride transfer step.^{204,205} Hammett studies were used to probe the electronic properties of active sites at metal–support interfaces by examining the slopes of linear Hammett relationships for Au on different supports.²⁰⁶ It was concluded that Au on TiO₂ and ZnO has more negatively charged interfacial Au sites than interfacial Au sites on Al₂O₃ and SiO₂.²⁰⁶ This provides a unique way to measure the electron density of interfacial sites.

Finally, our focus here was exclusively on oxide supports. Transition-metal carbides and nitrides have long attracted attention as potential replacements for Pt group catalysts,^{207,208} and recently it has been shown that they can be synthesized with high surface areas and exhibit unique properties as catalyst supports.^{209,210} For example, atypical shaped Pt particles (raft-like shaped) formed from strong interactions with the Mo₂C support exhibited higher activity in WGS than Al₂O₃, CeO₂, TiO₂-supported Pt and a commercial Cu–Zn–Al catalysts due to a high density of active sites at the perimeter of the Pt particles.¹⁴ Furthermore, a high-temperature self-assembly route was recently demonstrated to synthesize transition metal carbides nanoparticles coated with thickness-controllable mono- or heterometallic noble metals surface shells that exhibited high stability for highly dispersed metals and unique reactivity in electrocatalytic reactions.^{211,174,212–214} It is interesting to consider how much of what is known about metal–oxide support interactions will transfer to other supports, such as carbides or nitrides, or if new concepts, ideas, and opportunities for tuning catalytic properties of supported metals will be uncovered.

We end by commenting that in comparison to the wealth of knowledge and theoretical insights that exist into the inherent reactivity of metal and alloyed metal surfaces, our understanding of the influence of supports on metals is much less developed. However, it is clear that there is significant potential

in the exploitation of metal–support interfaces for driving chemistry that a metal could not do alone. While new synthetic methods will promote the identification of potentially useful interfacial catalytic properties, developing deeper understanding of the equivalence of various structures of interfaces is likely to help guide synthesis development through rational processes. Finally, interfaces are dynamic, both in the motion of the metal and support, and it is expected that *in situ* analysis and perhaps at some point ultrafast analysis may provide deeper insight into these phenomena.¹¹¹

■ AUTHOR INFORMATION

Corresponding Author

*E-mail: pchristopher@ucsb.edu.

ORCID

Phillip Christopher: 0000-0002-4898-5510

Notes

The authors declare no competing financial interest.

■ ACKNOWLEDGMENTS

P.C. acknowledges funding from the National Science Foundation through grants CHE-1301019 and CBET 1510697 and CBET-1554112 in support of these efforts. G.W. Graham is acknowledged for his thoughtful reading of the manuscript prior to submission.

■ REFERENCES

- (1) Tauster, S. J.; Fung, S. C.; Garten, R. L. Strong Metal-Support Interactions. Group 8 Noble Metals Supported on Titanium Dioxide. *J. Am. Chem. Soc.* **1978**, *100*, 170–175.
- (2) Pacchioni, G. Electronic Interactions and Charge Transfers of Metal Atoms and Clusters on Oxide Surfaces. *Phys. Chem. Chem. Phys.* **2013**, *15*, 1737–1757.
- (3) Pacchioni, G. Oxygen Vacancy: The Invisible Agent on Oxide Surfaces. *ChemPhysChem* **2003**, *4*, 1041–1047.
- (4) Munnik, P.; de Jongh, P. E.; de Jong, K. P. Recent Developments in the Synthesis of Supported Catalysts. *Chem. Rev.* **2015**, *115*, 6687–6718.
- (5) Rioux, R. M.; Song, H.; Hoefelmeyer, J. D.; Yang, P.; Somorjai, G. A. High-Surface-Area Catalyst Design: Synthesis, Characterization, and Reaction Studies of Platinum Nanoparticles in Mesoporous SBA-15 Silica. *J. Phys. Chem. B* **2005**, *109*, 2192–2202.
- (6) Tauster, S. J.; Fung, S. C.; Baker, R. T. K.; Horsley, J. A. Strong-Interactions in Supported-Metal Catalysis. *Science* **1981**, *211*, 1121–1125.
- (7) Haller, G. L.; Resasco, D. E. Metal–Support Interaction: Group VIII Metals and Reducible Oxides. In *Advances in Catalysis*; Eley, D. D., Pines, H., Weisz, P. B., Eds.; Academic Press, 1989; Vol. 36, pp 173–235.
- (8) Resasco, D. E.; Haller, G. L. A Model of Metal-Oxide Support Interaction for Rh on TiO₂. *J. Catal.* **1983**, *82*, 279–288.
- (9) Tauster, S. J. Strong Metal-Support Interactions. *Acc. Chem. Res.* **1987**, *20*, 389–394.
- (10) Corral Valero, M.; Raybaud, P.; Sautet, P. Influence of the Hydroxylation of γ-Al₂O₃ Surfaces on the Stability and Diffusion of Single Pd Atoms: A DFT Study. *J. Phys. Chem. B* **2006**, *110*, 1759–1767.
- (11) Hemmingson, S. L.; Campbell, C. T. Trends in Adhesion Energies of Metal Nanoparticles on Oxide Surfaces: Understanding Support Effects in Catalysis and Nanotechnology. *ACS Nano* **2017**, *11*, 1196–1203.
- (12) Jones, J.; Xiong, H.; DeLaRiva, A. T.; Peterson, E. J.; Pham, H.; Challa, S. R.; Qi, G.; Oh, S.; Wiebenga, M. H.; Pereira Hernández, X. I.; Wang, Y.; Datye, A. K. Thermally Stable Single-Atom Platinum-on-Ceria Catalysts via Atom Trapping. *Science* **2016**, *353*, 150–154.

- (13) Kwak, J. H.; Hu, J.; Mei, D.; Yi, C.-W.; Kim, D. H.; Peden, C. H. F.; Allard, L. F.; Szanyi, J. Coordinatively Unsaturated Al³⁺ Centers as Binding Sites for Active Catalyst Phases of Platinum on γ -Al₂O₃. *Science* **2009**, *325*, 1670–1673.
- (14) Schweitzer, N. M.; Schaidle, J. A.; Ezekoye, O. K.; Pan, X.; Linic, S.; Thompson, L. T. High Activity Carbide Supported Catalysts for Water Gas Shift. *J. Am. Chem. Soc.* **2011**, *133*, 2378–2381.
- (15) Hansen, K. H.; Worren, T.; Stempel, S.; Laegsgaard, E.; Baumer, M.; Freund, H. J.; Besenbacher, F.; Stensgaard, I. Palladium Nanocrystals on Al₂O₃: Structure and Adhesion Energy. *Phys. Rev. Lett.* **1999**, *83*, 4120–4123.
- (16) Henry, C. R. Surface Studies of Supported Model Catalysts. *Surf. Sci. Rep.* **1998**, *31*, 231–325.
- (17) Campbell, C. T. Ultrathin Metal Films and Particles on Oxide Surfaces: Structural, Electronic and Chemisorptive Properties. *Surf. Sci. Rep.* **1997**, *27*, 1–111.
- (18) Farmer, J. A.; Campbell, C. T. Ceria Maintains Smaller Metal Catalyst Particles by Strong Metal-Support Bonding. *Science* **2010**, *329*, 933–936.
- (19) Seemala, B.; Cai, C. M.; Kumar, R.; Wyman, C. E.; Christopher, P. Effects of Cu–Ni Bimetallic Catalyst Composition and Support on Activity, Selectivity, and Stability for Furfural Conversion to 2-Methylfuran. *ACS Sustainable Chem. Eng.* **2018**, *6*, 2152–2161.
- (20) Seemala, B.; Cai, C. M.; Wyman, C. E.; Christopher, P. Support Induced Control of Surface Composition in Cu–Ni/TiO₂ Catalysts Enables High Yield Co-Conversion of HMF and Furfural to Methylated Furans. *ACS Catal.* **2017**, *7*, 4070–4082.
- (21) Lykhach, Y.; Kozlov, S. M.; Skála, T.; Tovt, A.; Stetsovych, V.; Tsud, N.; Dvořák, F.; Johánek, V.; Neitzel, A.; Mysliveček, J.; Fabris, S.; Matolín, V.; Neyman, K. M.; Libuda, J. Counting Electrons on Supported Nanoparticles. *Nat. Mater.* **2016**, *15*, 284.
- (22) Zhang, J.; Wang, B.; Nikolla, E.; Medlin, J. W. Directing Reaction Pathways through Controlled Reactant Binding at Pd–TiO₂ Interfaces. *Angew. Chem.* **2017**, *129*, 6694–6698.
- (23) Gänzler, A. M.; Casapu, M.; Maurer, F.; Störmer, H.; Gerthsen, D.; Ferré, G.; Vernoux, P.; Bornmann, B.; Frahm, R.; Murzin, V.; Nachtegaal, M.; Votsmeier, M.; Grunwaldt, J.-D. Tuning the Pt/CeO₂ Interface by In Situ Variation of the Pt Particle Size. *ACS Catal.* **2018**, *8*, 4800–4811.
- (24) Huizinga, T.; Van Grondelle, J.; Prins, R. A Temperature Programmed Reduction Study of Pt on Al₂O₃ and TiO₂. *Appl. Catal.* **1984**, *10*, 199–213.
- (25) Bruix, A.; Migani, A.; Vayssilov, G. N.; Neyman, K. M.; Libuda, J.; Illas, F. Effects of Deposited Pt Particles on the Reducibility of CeO₂(111). *Phys. Chem. Chem. Phys.* **2011**, *13*, 11384–11392.
- (26) Zecevic, J.; Vanbutsele, G.; de Jong, K. P.; Martens, J. A. Nanoscale Intimacy in Bifunctional Catalysts for Selective Conversion of Hydrocarbons. *Nature* **2015**, *528*, 245.
- (27) Green, I. X.; Tang, W.; Neurock, M.; Yates, J. T. Spectroscopic Observation of Dual Catalytic Sites During Oxidation of CO on a Au/TiO₂ Catalyst. *Science* **2011**, *333*, 736–739.
- (28) Fu, Q.; Wagner, T. Interaction of Nanostructured Metal Overlays with Oxide Surfaces. *Surf. Sci. Rep.* **2007**, *62*, 431–498.
- (29) Jingyue, L. Advanced Electron Microscopy of Metal–Support Interactions in Supported Metal Catalysts. *ChemCatChem* **2011**, *3*, 934–948.
- (30) Ahmadi, M.; Mistry, H.; Roldan Cuenya, B. Tailoring the Catalytic Properties of Metal Nanoparticles via Support Interactions. *J. Phys. Chem. Lett.* **2016**, *7*, 3519–3533.
- (31) Bäumer, M.; Freund, H.-J. Metal Deposits on Well-Ordered Oxide Films. *Prog. Surf. Sci.* **1999**, *61*, 127–198.
- (32) An, K.; Alayoglu, S.; Musselwhite, N.; Plamthottam, S.; Melaet, G.; Lindeman, A. E.; Somorjai, G. A. Enhanced CO Oxidation Rates at the Interface of Mesoporous Oxides and Pt Nanoparticles. *J. Am. Chem. Soc.* **2013**, *135*, 16689–16696.
- (33) Liu, P.; Qin, R.; Fu, G.; Zheng, N. Surface Coordination Chemistry of Metal Nanomaterials. *J. Am. Chem. Soc.* **2017**, *139*, 2122–2131.
- (34) Winterbottom, W. L. Equilibrium Shape of a Small Particle in Contact with a Foreign Substrate. *Acta Metall.* **1967**, *15*, 303–310.
- (35) Enterkin, J. A.; Poeppelmeier, K. R.; Marks, L. D. Oriented Catalytic Platinum Nanoparticles on High Surface Area Strontium Titanate Nanocuboids. *Nano Lett.* **2011**, *11*, 993–997.
- (36) Boudart, M. Turnover Rates in Heterogeneous Catalysis. *Chem. Rev.* **1995**, *95*, 661–666.
- (37) Topsøe, H.; Topsøe, N.; Bohlbro, H.; Dumesic, J. A. Supported Iron Catalysts: Particle Size Dependence of Catalytic and Chemisorptive Properties. In *Studies in Surface Science and Catalysis*; Seivama, T., Tanabe, K., Eds.; Elsevier, 1981; Vol. 7, pp 247–265.
- (38) Taylor, H. S. A Theory of the Catalytic Surface. *Proc. R. Soc. London, Ser. A* **1925**, *108*, 105–111.
- (39) Dahl, S.; Logadottir, A.; Egeberg, R. C.; Larsen, J. H.; Chorkendorff, I.; Törnqvist, E.; Nørskov, J. K. Role of Steps in N₂ Activation on Ru(0001). *Phys. Rev. Lett.* **1999**, *83*, 1814–1817.
- (40) Hammer, B.; Nielsen, O. H.; Nørskov, J. K. Structure Sensitivity in Adsorption: CO Interaction with Stepped and Reconstructed Pt Surfaces. *Catal. Lett.* **1997**, *46*, 31–35.
- (41) Boudart, M.; McDonald, M. A. Structure Sensitivity of Hydrocarbon Synthesis from CO and H₂. *J. Phys. Chem.* **1984**, *88*, 2185–2195.
- (42) Iglesia, E.; Soled, S. L.; Fiato, R. A. Fischer–Tropsch Synthesis on Cobalt and Ruthenium - Metal Dispersion and Support Effects on Reaction - Rate and Selectivity. *J. Catal.* **1992**, *137*, 212–224.
- (43) Van Hardeveld, R.; Hartog, F. The Statistics of Surface Atoms and Surface Sites on Metal Crystals. *Surf. Sci.* **1969**, *15*, 189–230.
- (44) Shekhar, M.; Wang, J.; Lee, W. S.; Williams, W. D.; Kim, S. M.; Stach, E. A.; Miller, J. T.; Delgass, W. N.; Ribeiro, F. H. Size and Support Effects for the Water-Gas Shift Catalysis over Gold Nanoparticles Supported on Model Al₂O₃ and TiO₂. *J. Am. Chem. Soc.* **2012**, *134*, 4700–4708.
- (45) Kale, M. J.; Christopher, P. Utilizing Quantitative in Situ FTIR Spectroscopy To Identify Well-Coordinated Pt Atoms as the Active Site for CO Oxidation on Al₂O₃-Supported Pt Catalysts. *ACS Catal.* **2016**, *6*, 5599–5609.
- (46) Allian, A. D.; Takanabe, K.; Fujidala, K. L.; Hao, X.; Truex, T. J.; Cai, J.; Buda, C.; Neurock, M.; Iglesia, E. Chemisorption of CO and Mechanism of CO Oxidation on Supported Platinum Nanoclusters. *J. Am. Chem. Soc.* **2011**, *133*, 4498–4517.
- (47) Boudart, M.; Rumpf, F. The Catalytic-Oxidation of CO and Structure Insensitivity. *React. Kinet. Catal. Lett.* **1987**, *35*, 95–105.
- (48) Avanesian, T.; Dai, S.; Kale, M. J.; Graham, G. W.; Pan, X.; Christopher, P. Quantitative and Atomic-Scale View of CO-Induced Pt Nanoparticle Surface Reconstruction at Saturation Coverage via DFT Calculations Coupled with in Situ TEM and IR. *J. Am. Chem. Soc.* **2017**, *139*, 4551–4558.
- (49) Cargnello, M.; Doan-Nguyen, V. V. T.; Gordon, T. R.; Diaz, R. E.; Stach, E. A.; Gorte, R. J.; Fornasiero, P.; Murray, C. B. Control of Metal Nanocrystal Size Reveals Metal-Support Interface Role for Ceria Catalysts. *Science* **2013**, *341*, 771–773.
- (50) Bunluesin, T.; Putna, E. S.; Gorte, R. J. A Comparison of CO Oxidation on Ceria-Supported Pt, Pd, and Rh. *Catal. Lett.* **1996**, *41*, 1–5.
- (51) Widmann, D.; Liu, Y.; Schüth, F.; Behm, R. J. Support Effects in the Au-catalyzed CO oxidation – Correlation between Activity, Oxygen Storage Capacity, and Support Reducibility. *J. Catal.* **2010**, *276*, 292–305.
- (52) Michalak, W. D.; Krier, J. M.; Alayoglu, S.; Shin, J. Y.; An, K.; Komvopoulos, K.; Liu, Z.; Somorjai, G. A. CO Oxidation on PtSn Nanoparticle Catalysts Occurs at the Interface of Pt and Sn Oxide Domains Formed under Reaction Conditions. *J. Catal.* **2014**, *312*, 17–25.
- (53) Li, N.; Chen, Q.-Y.; Luo, L.-F.; Huang, W.-X.; Luo, M.-F.; Hu, G.-S.; Lu, J.-Q. Kinetic Study and the Effect of Particle Size on Low Temperature CO Oxidation over Pt/TiO₂ Catalysts. *Appl. Catal., B* **2013**, *142–143*, 523–532.
- (54) Bozo, C.; Guilhaume, N.; Herrmann, J.-M. Role of the Ceria-Zirconia Support in the Reactivity of Platinum and Palladium

- Catalysts for Methane Total Oxidation under Lean Conditions. *J. Catal.* **2001**, *203*, 393–406.
- (55) Pantu, P.; Gavalas, G. R. Methane Partial Oxidation on Pt/CeO₂ and Pt/Al₂O₃ Catalysts. *Appl. Catal., A* **2002**, *223*, 253–260.
- (56) Christian Enger, B.; Lødeng, R.; Holmen, A. A Review of Catalytic Partial Oxidation of Methane to Synthesis Gas with Emphasis on Reaction Mechanisms over Transition Metal Catalysts. *Appl. Catal., A* **2008**, *346*, 1–27.
- (57) Fierro-Gonzalez, J. C.; Gates, B. C. Mononuclear AuIII and AuI Complexes Bonded to Zeolite NaY: Catalysts for CO Oxidation at 298 K. *J. Phys. Chem. B* **2004**, *108*, 16999–17002.
- (58) Guzman, J.; Carrettin, S.; Fierro-Gonzalez, J. C.; Hao, Y.; Gates, B. C.; Corma, A. CO Oxidation Catalyzed by Supported Gold: Cooperation between Gold and Nanocrystalline Rare-Earth Supports Forms Reactive Surface Superoxide and Peroxide Species. *Angew. Chem., Int. Ed.* **2005**, *44*, 4778–4781.
- (59) Hutchings, G. J.; Hall, M. S.; Carley, A. F.; Landon, P.; Solsona, B. E.; Kiely, C. J.; Herzing, A.; Makkee, M.; Moulijn, J. A.; Overweg, A.; Fierro-Gonzalez, J. C.; Guzman, J.; Gates, B. C. Role of Gold Cations in the Oxidation of Carbon Monoxide Catalyzed by Iron Oxide-Supported Gold. *J. Catal.* **2006**, *242*, 71–81.
- (60) Concepción, P.; Carrettin, S.; Corma, A. Stabilization of Cationic Gold Species on Au/CeO₂ Catalysts under Working Conditions. *Appl. Catal., A* **2006**, *307*, 42–45.
- (61) Kotobuki, M.; Leppelt, R.; Hansgen, D. A.; Widmann, D.; Behm, R. J. Reactive Oxygen on a Au/TiO₂ Supported Catalyst. *J. Catal.* **2009**, *264*, 67–76.
- (62) Widmann, D.; Hocking, E.; Behm, R. J. On the Origin of the Selectivity in the Preferential CO Oxidation on Au/TiO₂ – Nature of the Active Oxygen Species for H₂ Oxidation. *J. Catal.* **2014**, *317*, 272–276.
- (63) Williams, W. D.; Shekhar, M.; Lee, W. S.; Kispersky, V.; Delgass, W. N.; Ribeiro, F. H.; Kim, S. M.; Stach, E. A.; Miller, J. T.; Allard, L. F. Metallic Corner Atoms in Gold Clusters Supported on Rutile Are the Dominant Active Site during Water-Gas Shift Catalysis. *J. Am. Chem. Soc.* **2010**, *132*, 14018–14020.
- (64) Fu, Q.; Saltsburg, H.; Flytzani-Stephanopoulos, M. Active Nonmetallic Au and Pt Species on Ceria-Based Water-Gas Shift Catalysts. *Science* **2003**, *301*, 935–938.
- (65) Foppa, L.; Margossian, T.; Kim, S. M.; Müller, C.; Copéret, C.; Larmier, K.; Comas-Vives, A. Contrasting the Role of Ni/Al₂O₃ Interfaces in Water–Gas Shift and Dry Reforming of Methane. *J. Am. Chem. Soc.* **2017**, *139*, 17128–17139.
- (66) Bunluesin, T.; Cordatos, H.; Gorte, R. J. Study of CO Oxidation Kinetics on Rh/Ceria. *J. Catal.* **1995**, *157*, 222–226.
- (67) Zafiris, G. S.; Gorte, R. J. Evidence for a Second CO Oxidation Mechanism on Rh/Ceria. *J. Catal.* **1993**, *143*, 86–91.
- (68) Ojeda, M.; Zhan, B.-Z.; Iglesia, E. Mechanistic Interpretation of CO Oxidation Turnover Rates on Supported Au Clusters. *J. Catal.* **2012**, *285*, 92–102.
- (69) Saavedra, J.; Doan, H. A.; Pursell, C. J.; Grabow, L. C.; Chandler, B. D. The Critical Role of Water at the Gold-Titania Interface in Catalytic CO Oxidation. *Science* **2014**, *345*, 1599–1602.
- (70) Saavedra, J.; Pursell, C. J.; Chandler, B. D. CO Oxidation Kinetics over Au/TiO₂ and Au/Al₂O₃ Catalysts: Evidence for a Common Water-Assisted Mechanism. *J. Am. Chem. Soc.* **2018**, *140*, 3712–3723.
- (71) Kale, M. J.; Gidcumb, D.; Gulian, F. J.; Miller, S. P.; Clark, C. H.; Christopher, P. Evaluation of Platinum Catalysts for Naval Submarine Pollution Control. *Appl. Catal., B* **2017**, *203*, 533–540.
- (72) Yamada, Y.; Tsung, C.-K.; Huang, W.; Huo, Z.; Habas, S. E.; Soejima, T.; Aliaga, C. E.; Somorjai, G. A.; Yang, P. Nanocrystal Bilayer for Tandem Catalysis. *Nat. Chem.* **2011**, *3*, 372.
- (73) Yang, X.; Mueangnern, Y.; Baker, Q. A.; Baker, L. R. Crotonaldehyde Hydrogenation on Platinum-Titanium Oxide and Platinum-Cerium Oxide Catalysts: Selective C[double bond, length as m-dash]O Bond Hydrogen Requires Platinum Sites beyond the Oxide-Metal Interface. *Catal. Sci. Technol.* **2016**, *6*, 6824–6835.
- (74) Kattel, S.; Liu, P.; Chen, J. G. G. Tuning Selectivity of CO₂ Hydrogenation Reactions at the Metal/Oxide Interface. *J. Am. Chem. Soc.* **2017**, *139*, 9739–9754.
- (75) Su, J.; Xie, C.; Chen, C.; Yu, Y.; Kennedy, G.; Somorjai, G. A.; Yang, P. Insights into the Mechanism of Tandem Alkene Hydroformylation over a Nanostructured Catalyst with Multiple Interfaces. *J. Am. Chem. Soc.* **2016**, *138*, 11568–11574.
- (76) Kattel, S.; Yan, B.; Chen, J. G.; Liu, P. CO₂ Hydrogenation on Pt, Pt/SiO₂ and Pt/TiO₂: Importance of Synergy between Pt and Oxide Support. *J. Catal.* **2016**, *343*, 115–126.
- (77) Mehta, P.; Greeley, J.; Delgass, W. N.; Schneider, W. F. Adsorption Energy Correlations at the Metal–Support Boundary. *ACS Catal.* **2017**, *7*, 4707–4715.
- (78) Kumar, G.; Nikolla, E.; Linic, S.; Medlin, J. W.; Janik, M. J. Multicomponent Catalysts: Limitations and Prospects. *ACS Catal.* **2018**, *8*, 3202–3208.
- (79) Andersen, M.; Medford, A. J.; Nørskov, J. K.; Reuter, K. Analyzing the Case for Bifunctional Catalysis. *Angew. Chem., Int. Ed.* **2016**, *55*, 5210–5214.
- (80) Andersen, M.; Medford, A. J.; Nørskov, J. K.; Reuter, K. Scaling-Relation-Based Analysis of Bifunctional Catalysis: The Case for Homogeneous Bimetallic Alloys. *ACS Catal.* **2017**, *7*, 3960–3967.
- (81) Ammal, S. C.; Heyden, A. Nature of Pt/TiO₂(110) Interface under Water-Gas Shift Reaction Conditions: A Constrained ab Initio Thermodynamics Study. *J. Phys. Chem. C* **2011**, *115*, 19246–19259.
- (82) Molina, L. M.; Hammer, B. Active Role of Oxide Support during CO Oxidation at Au/MgO. *Phys. Rev. Lett.* **2003**, *90*, 206102.
- (83) Green, I. X.; Tang, W.; Neurock, M.; Yates, J. T. Low-Temperature Catalytic H₂ Oxidation over Au Nanoparticle/TiO₂ Dual Perimeter Sites. *Angew. Chem., Int. Ed.* **2011**, *50*, 10186–10189.
- (84) Duan, Z.; Henkelman, G. CO Oxidation at the Au/TiO₂ Boundary: The Role of the Au/TiSc Site. *ACS Catal.* **2015**, *5*, 1589–1595.
- (85) Kozlov, S. M.; Neyman, K. M. Effects of Electron Transfer in Model Catalysts Composed of Pt Nanoparticles on CeO₂(111) Surface. *J. Catal.* **2016**, *344*, 507–514.
- (86) Lin, X.; Nilius, N.; Sterrer, M.; Koskinen, P.; Hakkinen, H.; Freund, H. J. Characterizing Low-Coordinated Atoms at the Periphery of MgO-Supported Au Islands using Scanning Tunneling Microscopy and Electronic Structure Calculations. *Phys. Rev. B: Condens. Matter Mater. Phys.* **2010**, *81*, 153406.
- (87) Lin, X.; Yang, B.; Benia, H. M.; Myrach, P.; Yulikov, M.; Aumer, A.; Brown, M. A.; Sterrer, M.; Bondarchuk, O.; Kieseritzky, E.; Rocker, J.; Rissee, T.; Gao, H. J.; Nilius, N.; Freund, H. J. Charge-Mediated Adsorption Behavior of CO on MgO-Supported Au Clusters. *J. Am. Chem. Soc.* **2010**, *132*, 7745–7749.
- (88) Meier, D. C.; Goodman, D. W. The Influence of Metal Cluster Size on Adsorption Energies: CO Adsorbed on Au Clusters Supported on TiO₂. *J. Am. Chem. Soc.* **2004**, *126*, 1892–1899.
- (89) Lu, J.; Serna, P.; Aydin, C.; Browning, N. D.; Gates, B. C. Supported Molecular Iridium Catalysts: Resolving Effects of Metal Nuclearity and Supports as Ligands. *J. Am. Chem. Soc.* **2011**, *133*, 16186–16195.
- (90) Argo, A. M.; Odzak, J. F.; Lai, F. S.; Gates, B. C. Observation of Ligand Effects during Alkene Hydrogenation Catalysed by Supported Metal Clusters. *Nature* **2002**, *415*, 623.
- (91) Li, L.; Larsen, A. H.; Romero, N. A.; Morozov, V. A.; Glinsvad, C.; Abild-Pedersen, F.; Greeley, J.; Jacobsen, K. W.; Nørskov, J. K. Investigation of Catalytic Finite-Size-Effects of Platinum Metal Clusters. *J. Phys. Chem. Lett.* **2013**, *4*, 222–226.
- (92) Li, T.; Liu, F.; Tang, Y.; Li, L.; Miao, S.; Su, Y.; Zhang, J.; Huang, J.; Sun, H.; Haruta, M.; Wang, A.; Qiao, B.; Li, J.; Zhang, T. Maximizing Interfacial Sites by Single-Atom Catalyst for Solvent-Free Selective Oxidation of Primary Alcohol. *Angew. Chem.* **2018**, *130*, 7921–7925.
- (93) Ruiz Puigdollers, A.; Schlexer, P.; Tosoni, S.; Pacchioni, G. Increasing Oxide Reducibility: The Role of Metal/Oxide Interfaces in the Formation of Oxygen Vacancies. *ACS Catal.* **2017**, *7*, 6493–6513.

- (94) Ammal, S. C.; Heyden, A. Modeling the Noble Metal/TiO₂ Interface with Hybrid DFT Functionals: A Periodic Electrostatic Embedded Cluster Model Study. *J. Chem. Phys.* **2010**, *133*, 164703.
- (95) Sun, Y. N.; Giordano, L.; Goniakowski, J.; Lewandowski, M.; Qin, Z. H.; Noguera, C.; Shaikhutdinov, S.; Pacchioni, G.; Freund, H. J. The Interplay between Structure and CO Oxidation Catalysis on Metal-Supported Ultrathin Oxide Films. *Angew. Chem., Int. Ed.* **2010**, *49*, 4418–4421.
- (96) Zhao, K.; Tang, H.; Qiao, B.; Li, L.; Wang, J. High Activity of Au/γ-Fe₂O₃ for CO Oxidation: Effect of Support Crystal Phase in Catalyst Design. *ACS Catal.* **2015**, *5*, 3528–3539.
- (97) Vayssilov, G. N.; Lykhach, Y.; Migani, A.; Staudt, T.; Petrova, G. P.; Tsud, N.; Skála, T.; Bruix, A.; Illas, F.; Prince, K. C.; Matolín, V. r.; Neyman, K. M.; Libuda, J. Support Nanostructure Boosts Oxygen Transfer to Catalytically Active Platinum Nanoparticles. *Nat. Mater.* **2011**, *10*, 310.
- (98) Saqlain, M. A.; Hussain, A.; Siddiq, M.; Ferreira, A. R.; Leitao, A. A. Thermally Activated Surface Oxygen Defects at the Perimeter of Au/TiO₂: a DFT+U Study. *Phys. Chem. Chem. Phys.* **2015**, *17*, 25403–25410.
- (99) Tyo, E. C.; Vajda, S. Catalysis by Clusters with Precise Numbers of Atoms. *Nat. Nanotechnol.* **2015**, *10*, 577.
- (100) Kaden, W. E.; Wu, T.; Kunkel, W. A.; Anderson, S. L. Electronic Structure Controls Reactivity of Size-Selected Pd Clusters Adsorbed on TiO₂ Surfaces. *Science* **2009**, *326*, 826–829.
- (101) Abbet, S.; Sanchez, A.; Heiz, U.; Schneider, W. D.; Ferrari, A. M.; Pacchioni, G.; Rösch, N. Acetylene Cyclotrimerization on Supported Size-Selected Pdn Clusters ($1 \leq n \leq 30$): One Atom Is Enough! *J. Am. Chem. Soc.* **2000**, *122*, 3453–3457.
- (102) Sanchez, A.; Abbet, S.; Heiz, U.; Schneider, W. D.; Häkkinen, H.; Barnett, R. N.; Landman, U. When Gold Is Not Noble: Nanoscale Gold Catalysts. *J. Phys. Chem. A* **1999**, *103*, 9573–9578.
- (103) Zhai, H.; Alexandrova, A. N. Local Fluxionality of Surface-Deposited Cluster Catalysts: The Case of Pt₇ on Al₂O₃. *J. Phys. Chem. Lett.* **2018**, *9*, 1696–1702.
- (104) Baxter, E. T.; Ha, M.-A.; Cass, A. C.; Alexandrova, A. N.; Anderson, S. L. Ethylene Dehydrogenation on Pt_{4,7,8} Clusters on Al₂O₃: Strong Cluster Size Dependence Linked to Preferred Catalyst Morphologies. *ACS Catal.* **2017**, *7*, 3322–3335.
- (105) Zhai, H.; Alexandrova, A. N. Fluxionality of Catalytic Clusters: When It Matters and How to Address It. *ACS Catal.* **2017**, *7*, 1905–1911.
- (106) Sun, G.; Sautet, P. Metastable Structures in Cluster Catalysis from First-Principles: Structural Ensemble in Reaction Conditions and Metastability Triggered Reactivity. *J. Am. Chem. Soc.* **2018**, *140*, 2812–2820.
- (107) Bruix, A.; Rodriguez, J. A.; Ramírez, P. J.; Senanayake, S. D.; Evans, J.; Park, J. B.; Stacchiola, D.; Liu, P.; Hrbek, J.; Illas, F. A New Type of Strong Metal–Support Interaction and the Production of H₂ through the Transformation of Water on Pt/CeO₂(111) and Pt/CeO_x/TiO₂(110) Catalysts. *J. Am. Chem. Soc.* **2012**, *134*, 8968–8974.
- (108) DeRita, L.; Dai, S.; Lopez-Zepeda, K.; Pham, N.; Graham, G. W.; Pan, X.; Christopher, P. Catalyst Architecture for Stable Single Atom Dispersion Enables Site-Specific Spectroscopic and Reactivity Measurements of CO Adsorbed to Pt Atoms, Oxidized Pt Clusters, and Metallic Pt Clusters on TiO₂. *J. Am. Chem. Soc.* **2017**, *139*, 14150–14165.
- (109) Pacchioni, G.; Freund, H.-J. Controlling the Charge State of Supported Nanoparticles in Catalysis: Lessons from Model Systems. *Chem. Soc. Rev.* **2018**, in press, DOI: 10.1039/C8CS00152A.
- (110) Liu, J.-C.; Wang, Y.-G.; Li, J. Toward Rational Design of Oxide-Supported Single-Atom Catalysts: Atomic Dispersion of Gold on Ceria. *J. Am. Chem. Soc.* **2017**, *139*, 6190–6199.
- (111) Wang, Y.-G.; Mei, D.; Glezakou, V.-A.; Li, J.; Rousseau, R. Dynamic Formation of Single-Atom Catalytic Active Sites on Ceria-Supported Gold Nanoparticles. *Nat. Commun.* **2015**, *6*, 6511.
- (112) Bernal, S.; Calvino, J. J.; Cauqui, M. A.; Gatica, J. M.; López Cartes, C.; Pérez Omil, J. A.; Pintado, J. M. Some Contributions of Electron Microscopy to the Characterisation of the Strong Metal–Support Interaction Effect. *Catal. Today* **2003**, *77*, 385–406.
- (113) Shi, X. Y.; Zhang, W.; Zhang, C.; Zheng, W. T.; Chen, H.; Qi, J. G. Real-Space Observation of Strong Metal-Support Interaction: State-of-the-Art and What's the Next. *J. Microsc.* **2016**, *262*, 203–215.
- (114) Zhang, S.; Plessow, P. N.; Willis, J. J.; Dai, S.; Xu, M.; Graham, G. W.; Cargnello, M.; Abild-Pedersen, F.; Pan, X. Dynamical Observation and Detailed Description of Catalysts under Strong Metal–Support Interaction. *Nano Lett.* **2016**, *16*, 4528–4534.
- (115) Matsubu, J. C.; Zhang, S. Y.; DeRita, L.; Marinkovic, N. S.; Chen, J. G. G.; Graham, G. W.; Pan, X. Q.; Christopher, P. Adsorbate-Mediated Strong Metal-Support Interactions in Oxide-Supported Rh Catalysts. *Nat. Chem.* **2017**, *9*, 120–127.
- (116) Lunkenbein, T.; Schumann, J.; Behrens, M.; Schlogl, R.; Willinger, M. G. Formation of a ZnO Overlayer in Industrial Cu/ZnO/Al₂O₃ Catalysts Induced by Strong Metal–Support Interactions. *Angew. Chem.* **2015**, *127*, 4627–4631.
- (117) Ta, N.; Liu, J.; Chenna, S.; Crozier, P. A.; Li, Y.; Chen, A.; Shen, W. Stabilized Gold Nanoparticles on Ceria Nanorods by Strong Interfacial Anchoring. *J. Am. Chem. Soc.* **2012**, *134*, 20585–20588.
- (118) Tao, F.; Crozier, P. A. Atomic-Scale Observations of Catalyst Structures under Reaction Conditions and during Catalysis. *Chem. Rev.* **2016**, *116*, 3487–3539.
- (119) Gao, W.; Hood, Z. D.; Chi, M. Interfaces in Heterogeneous Catalysts: Advancing Mechanistic Understanding through Atomic-Scale Measurements. *Acc. Chem. Res.* **2017**, *50*, 787–795.
- (120) Barcaro, G.; Agnoli, S.; Sedona, F.; Rizzi, G. A.; Fortunelli, A.; Granozzi, G. Structure of Reduced Ultrathin TiOx Polar Films on Pt(111). *J. Phys. Chem. C* **2009**, *113*, 5721–5729.
- (121) Belton, D. N.; Sun, Y. M.; White, J. M. Metal-Support Interactions on Rhodium and Platinum/Titanium Dioxide Model Catalysts. *J. Phys. Chem.* **1984**, *88*, 5172–5176.
- (122) Dulub, O.; Hebenstreit, W.; Diebold, U. Imaging Cluster Surfaces with Atomic Resolution: The Strong Metal-Support Interaction State of Pt Supported on TiO_2 . *Phys. Rev. Lett.* **2000**, *84*, 3646–3649.
- (123) Iddir, H.; Disko, M. M.; Ogut, S.; Browning, N. D. Atomic Scale Characterization of the Pt/TiO₂ Interface. *Micron* **2005**, *36*, 233–241.
- (124) Sun, Y. M.; Belton, D. N.; White, J. M. Characteristics of Platinum Thin Films on Titanium Dioxide(110). *J. Phys. Chem.* **1986**, *90*, 5178–5182.
- (125) Pesty, F.; Steinrück, H.-P.; Madey, T. E. Thermal Stability of Pt Films on TiO₂(110): Evidence for Encapsulation. *Surf. Sci.* **1995**, *339*, 83–95.
- (126) Ozturk, O.; Park, J. B.; Ma, S.; Ratliff, J. S.; Zhou, J.; Mullins, D. R.; Chen, D. A. Probing the Interactions of Pt, Rh and Bimetallic Pt–Rh Clusters with the TiO₂(110) Support. *Surf. Sci.* **2007**, *601*, 3099–3113.
- (127) Bardi, U.; Tamura, K.; Nihei, Y. Effect of High Temperature Reduction in Hydrogen on Pt Deposited on the TiO₂(100) Surface: An Angle Resolved X-ray Photoemission Study. *Catal. Lett.* **1989**, *3*, 117–128.
- (128) Willinger, M. G.; Zhang, W.; Bondarchuk, O.; Shaikhutdinov, S.; Freund, H.-J.; Schlögl, R. A Case of Strong Metal–Support Interactions: Combining Advanced Microscopy and Model Systems to Elucidate the Atomic Structure of Interfaces. *Angew. Chem., Int. Ed.* **2014**, *53*, 5998–6001.
- (129) Dai, S.; Gao, W. P.; Zhang, S. Y.; Graham, G. W.; Pan, X. Q. Transmission Electron Microscopy with Atomic Resolution under Atmospheric Pressures. *MRS Commun.* **2017**, *7*, 798–812.
- (130) Braunschweig, E. J.; Logan, A. D.; Datye, A. K.; Smith, D. J. Reversibility of Strong Metal-Support Interactions on RhTiO₂. *J. Catal.* **1989**, *118*, 227–237.
- (131) Williams, K. J.; Levin, M. E.; Salmeron, M.; Bell, A. T.; Somorjai, G. A. Ethylene Hydrogenation and Ethane Hydrogenolysis on a Rh Foil with Titania Overlays. *Catal. Lett.* **1988**, *1*, 331–338.

- (132) Sinfelt, J. H.; Carter, J. L.; Yates, D. J. C. Catalytic Hydrogenolysis and Dehydrogenation over Copper-Nickel Alloys. *J. Catal.* **1972**, *24*, 283–296.
- (133) Pan, Q.; Liu, B. H.; McBriarty, M. E.; Martynova, Y.; Groot, I. M. N.; Wang, S.; Bedzyk, M. J.; Shaikhutdinov, S.; Freund, H.-J. Reactivity of Ultra-Thin ZnO Films Supported by Ag(111) and Cu(111): A Comparison to ZnO/Pt(111). *Catal. Lett.* **2014**, *144*, 648–655.
- (134) Schott, V.; Oberhofer, H.; Birkner, A.; Xu, M. C.; Wang, Y. M.; Muhler, M.; Reuter, K.; Woll, C. Chemical Activity of Thin Oxide Layers: Strong Interactions with the Support Yield a New Thin-Film Phase of ZnO. *Angew. Chem., Int. Ed.* **2013**, *52*, 11925–11929.
- (135) Dandekar, A.; Vannice, M. A. Crotonaldehyde Hydrogenation on Pt/TiO₂ and Ni/TiO₂ SMSI Catalysts. *J. Catal.* **1999**, *183*, 344–354.
- (136) Zanella, R.; Louis, C.; Giorgio, S.; Touroude, R. Crotonaldehyde Hydrogenation by Gold Supported on TiO₂: Structure Sensitivity and Mechanism. *J. Catal.* **2004**, *223*, 328–339.
- (137) Rodriguez, J. A.; Liu, P.; Stacchiola, D. J.; Senanayake, S. D.; White, M. G.; Chen, J. G. Hydrogenation of CO₂ to Methanol: Importance of Metal–Oxide and Metal–Carbide Interfaces in the Activation of CO₂. *ACS Catal.* **2015**, *5*, 6696–6706.
- (138) Behrens, M.; Studt, F.; Kasatkina, I.; Kuhl, S.; Havecker, M.; Abild-Pedersen, F.; Zander, S.; Girgsdies, F.; Kurr, P.; Kniep, B. L.; Tovar, M.; Fischer, R. W.; Norskov, J. K.; Schlogl, R. The Active Site of Methanol Synthesis over Cu/ZnO/Al₂O₃ Industrial Catalysts. *Science* **2012**, *336*, 893–897.
- (139) Graciani, J.; Mudiyanselage, K.; Xu, F.; Baber, A. E.; Evans, J.; Senanayake, S. D.; Stacchiola, D. J.; Liu, P.; Hrbek, J.; Sanz, J. F.; Rodriguez, J. A. Highly Active Copper-Ceria and Copper-Ceria-Titania Catalysts for Methanol Synthesis from CO₂. *Science* **2014**, *345*, 546–550.
- (140) Kattel, S.; Ramírez, P. J.; Chen, J. G.; Rodriguez, J. A.; Liu, P. Active Sites for CO₂ Hydrogenation to Methanol on Cu/ZnO Catalysts. *Science* **2017**, *355*, 1296–1299.
- (141) Song, K.; Sauter, D. J.; Wu, J.; Dravid, V. P.; Stair, P. C. Evolution of High-Energy Electron Beam Irradiation Effects on Zeolite Supported Catalyst: Metal Nanoprecipitation. *ACS Catal.* **2012**, *2*, 384–390.
- (142) Pham, T.; Gibb, A. L.; Li, Z.; Gilbert, S. M.; Song, C.; Louie, S. G.; Zettl, A. Formation and Dynamics of Electron-Irradiation-Induced Defects in Hexagonal Boron Nitride at Elevated Temperatures. *Nano Lett.* **2016**, *16*, 7142–7147.
- (143) Krasheninnikov, A. V.; Nordlund, K. Ion and Electron Irradiation-Induced Effects in Nanostructured Materials. *J. Appl. Phys.* **2010**, *107*, 071301.
- (144) Resasco, J.; Dai, S.; Graham, G. W.; Pan, X.; Christopher, P., Combining In-situ Transmission Electron Microscopy and Infrared Spectroscopy for Understanding Dynamic and Atomic Scale Features of Supported Metal Catalysts. *J. Phys. Chem. C* **2018**, in press, DOI: 10.1021/acs.jpcc.8b03959.
- (145) Hayek, K.; Fuchs, M.; Klotzer, B.; Reichl, W.; Rupprechter, G. Studies of Metal-Support Interactions with “Real” and “Inverted” Model Systems: Reactions of CO and Small Hydrocarbons with Hydrogen on Noble Metals in Contact with Oxides. *Top. Catal.* **2000**, *13*, 55–66.
- (146) Ladas, S.; Poppa, H.; Boudart, M. The Adsorption and Catalytic-Oxidation of Carbon-Monoxide on Evaporated Palladium Particles. *Surf. Sci.* **1981**, *102*, 151–171.
- (147) Rumpf, F.; Poppa, H.; Boudart, M. Oxidation of Carbon Monoxide on Palladium: Role of the Alumina Support. *Langmuir* **1988**, *4*, 722–728.
- (148) Boffa, A.; Lin, C.; Bell, A. T.; Somorjai, G. A. Promotion of CO and CO₂ Hydrogenation over Rh by Metal Oxides: The Influence of Oxide Lewis Acidity and Reducibility. *J. Catal.* **1994**, *149*, 149–158.
- (149) Levin, M. E.; Williams, K. J.; Salmeron, M.; Bell, A. T.; Somorjai, G. A. Alumina and Titania Overlayers on Rhodium: A Comparison of the Chemisorption Catalytic Properties. *Surf. Sci.* **1988**, *195*, 341–351.
- (150) Levin, M.; Salmeron, M.; Bell, A. T.; Somorjai, G. A. The Influence of TiO_x Deposits on a Polycrystalline Rh Foil on CO Adsorption and Deposition. *Surf. Sci.* **1986**, *169*, 123–137.
- (151) Levin, M. E.; Salmeron, M.; Bell, A. T.; Somorjai, G. A. The Enhancement of CO Hydrogenation on Rhodium by TiO_x Overlays. *J. Catal.* **1987**, *106*, 401–409.
- (152) Rodriguez, J. A.; Liu, P.; Graciani, J.; Senanayake, S. D.; Grinter, D. C.; Stacchiola, D.; Hrbek, J.; Fernández-Sanz, J. Inverse Oxide/Metal Catalysts in Fundamental Studies and Practical Applications: A Perspective of Recent Developments. *J. Phys. Chem. Lett.* **2016**, *7*, 2627–2639.
- (153) Guo, Y.; Zhang, Y.-W. Metal Clusters Dispersed on Oxide Supports: Preparation Methods and Metal-Support Interactions. *Top. Catal.* **2018**, *61*, 855–874.
- (154) Sun, Y. N.; Qin, Z. H.; Lewandowski, M.; Carrasco, E.; Sterrer, M.; Shaikhutdinov, S.; Freund, H. J. Monolayer Iron Oxide Film on Platinum Promotes Low Temperature CO Oxidation. *J. Catal.* **2009**, *266*, 359–368.
- (155) Rodriguez, J. A.; Ma, S.; Liu, P.; Hrbek, J.; Evans, J.; Perez, M. Activity of CeO_x and TiO_x Nanoparticles Grown on Au(111) in the Water-Gas Shift Reaction. *Science* **2007**, *318*, 1757–1760.
- (156) Suchorski, Y.; Wrobel, R.; Becker, S.; Weiss, H. CO Oxidation on a CeO_x/Pt(111) Inverse Model Catalyst Surface: Catalytic Promotion and Tuning of Kinetic Phase Diagrams. *J. Phys. Chem. C* **2008**, *112*, 20012–20017.
- (157) Nakamura, I.; Mantoku, H.; Furukawa, T.; Fujitani, T. Active Sites for Hydrogen Dissociation over TiO_x/Au(111) Surfaces. *J. Phys. Chem. C* **2011**, *115*, 16074–16080.
- (158) Hornés, A.; Hungría, A. B.; Bera, P.; Cámaras, A. L.; Fernández-García, M.; Martínez-Arias, A.; Barrio, L.; Estrella, M.; Zhou, G.; Fonseca, J. J.; Hanson, J. C.; Rodriguez, J. A. Inverse CeO₂/CuO Catalyst As an Alternative to Classical Direct Configurations for Preferential Oxidation of CO in Hydrogen-Rich Stream. *J. Am. Chem. Soc.* **2010**, *132*, 34–35.
- (159) Lunkenbein, T.; Schumann, J.; Behrens, M.; Schlogl, R.; Willinger, M. G. Formation of a ZnO Overlayer in Industrial Cu/ZnO/Al₂O₃ Catalysts Induced by Strong Metal-Support Interactions. *Angew. Chem., Int. Ed.* **2015**, *54*, 4544–4548.
- (160) Fu, Q.; Li, W. X.; Yao, Y. X.; Liu, H. Y.; Su, H. Y.; Ma, D.; Gu, X. K.; Chen, L. M.; Wang, Z.; Zhang, H.; Wang, B.; Bao, X. H. Interface-Confining Ferrous Centers for Catalytic Oxidation. *Science* **2010**, *328*, 1141–1144.
- (161) Ning, Y.; Wei, M.; Yu, L.; Yang, F.; Chang, R.; Liu, Z.; Fu, Q.; Bao, X. Nature of Interface Confinement Effect in Oxide/Metal Catalysts. *J. Phys. Chem. C* **2015**, *119*, 27556–27561.
- (162) Boudart, M. Model Catalysts: Reductionism for Understanding. *Top. Catal.* **2000**, *13*, 147–149.
- (163) Ramachandran, R. K.; Detavernier, C.; Dendooven, J. Atomic Layer Deposition for Catalysis. *Nanotechnology in Catalysis*; Wiley-VCH Verlag GmbH & Co. KGaA: Weinheim, 2017; pp 335–358.
- (164) Singh, J. A.; Yang, N.; Bent, S. F. Nanoengineering Heterogeneous Catalysts by Atomic Layer Deposition. *Annu. Rev. Chem. Biomol. Eng.* **2017**, *8*, 41–62.
- (165) Lu, J.; Fu, B.; Kung, M. C.; Xiao, G.; Elam, J. W.; Kung, H. H.; Stair, P. C. Coking- and Sintering-Resistant Palladium Catalysts Achieved Through Atomic Layer Deposition. *Science* **2012**, *335*, 1205–1208.
- (166) O’Neill, B. J.; Jackson, D. H. K.; Crisci, A. J.; Farberow, C. A.; Shi, F.; Alba-Rubio, A. C.; Lu, J.; Dietrich, P. J.; Gu, X.; Marshall, C. L.; Stair, P. C.; Elam, J. W.; Miller, J. T.; Ribeiro, F. H.; Voyles, P. M.; Greeley, J.; Mavrikakis, M.; Scott, S. L.; Kuech, T. F.; Dumesic, J. A. Stabilization of Copper Catalysts for Liquid-Phase Reactions by Atomic Layer Deposition. *Angew. Chem., Int. Ed.* **2013**, *52*, 13808–13812.
- (167) Lee, J. C.; Jackson, D. H. K.; Li, T.; Winans, R. E.; Dumesic, J. A.; Kuech, T. F.; Huber, G. W. Enhanced Stability of Cobalt Catalysts

- by Atomic Layer Deposition for Aqueous-Phase Reactions. *Energy Environ. Sci.* **2014**, *7*, 1657–1660.
- (168) Onn, T. M.; Zhang, S.; Arroyo-Ramirez, L.; Chung, Y.-C.; Graham, G. W.; Pan, X.; Gorte, R. J. Improved Thermal Stability and Methane-Oxidation Activity of Pd/Al₂O₃ Catalysts by Atomic Layer Deposition of ZrO₂. *ACS Catal.* **2015**, *5*, 5696–5701.
- (169) Feng, H.; Lu, J. L.; Stair, P. C.; Elam, J. W. Alumina Overcoating on Pd Nanoparticle Catalysts by Atomic Layer Deposition: Enhanced Stability and Reactivity. *Catal. Lett.* **2011**, *141*, 512–517.
- (170) Zhang, H. B.; Lei, Y.; Kropf, A. J.; Zhang, G. H.; Elam, J. W.; Miller, J. T.; Sollberger, F.; Ribeiro, F.; Akatay, M. C.; Stach, E. A.; Dumesic, J. A.; Marshall, C. L. Enhancing the Stability of Copper Chromite Catalysts for the Selective Hydrogenation of Furfural using ALD Overcoating. *J. Catal.* **2014**, *317*, 284–292.
- (171) Yang, N.; Yoo, J. S.; Schumann, J.; Bothra, P.; Singh, J. A.; Valle, E.; Abild-Pedersen, F.; Norskov, J. K.; Bent, S. F. Rh-MnO Interface Sites Formed by Atomic Layer Deposition Promote Syngas Conversion to Higher Oxygenates. *ACS Catal.* **2017**, *7*, 5746–5757.
- (172) Singh, J. A.; Thissen, N. F. W.; Kim, W.-H.; Johnson, H.; Kessels, W. M. M.; Bol, A. A.; Bent, S. F.; Mackus, A. J. M. Area-Selective Atomic Layer Deposition of Metal Oxides on Noble Metals through Catalytic Oxygen Activation. *Chem. Mater.* **2018**, *30*, 663–670.
- (173) Zhang, Q.; Lee, I.; Joo, J. B.; Zaera, F.; Yin, Y. Core–Shell Nanostructured Catalysts. *Acc. Chem. Res.* **2013**, *46*, 1816–1824.
- (174) Park, J.-N.; Forman, A. J.; Tang, W.; Cheng, J.; Hu, Y.-S.; Lin, H.; McFarland, E. W. Highly Active and Sinter-Resistant Pd-Nanoparticle Catalysts Encapsulated in Silica. *Small* **2008**, *4*, 1694–1697.
- (175) Joo, S. H.; Park, J. Y.; Tsung, C. K.; Yamada, Y.; Yang, P. D.; Somorjai, G. A. Thermally Stable Pt/Mesoporous Silica Core–Shell Nanocatalysts for High-Temperature Reactions. *Nat. Mater.* **2009**, *8*, 126–131.
- (176) An, K.; Zhang, Q.; Alayoglu, S.; Musselwhite, N.; Shin, J.-Y.; Somorjai, G. A. High-Temperature Catalytic Reforming of n-Hexane over Supported and Core–Shell Pt Nanoparticle Catalysts: Role of Oxide–Metal Interface and Thermal Stability. *Nano Lett.* **2014**, *14*, 4907–4912.
- (177) Adijanto, L.; Bennett, D. A.; Chen, C.; Yu, A. S.; Cargnello, M.; Fornasiero, P.; Gorte, R. J.; Vohs, J. M. Exceptional Thermal Stability of Pd@CeO₂ Core–Shell Catalyst Nanostructures Grafted onto an Oxide Surface. *Nano Lett.* **2013**, *13*, 2252–2257.
- (178) Gounder, R.; Iglesia, E. The Catalytic Diversity of Zeolites: Confinement and Solvation Effects within Voids of Molecular Dimensions. *Chem. Commun.* **2013**, *49*, 3491–3509.
- (179) Canlas, C. P.; Lu, J.; Ray, N. A.; Grosso-Giordano, N. A.; Lee, S.; Elam, J. W.; Winans, R. E.; Van Duyne, R. P.; Stair, P. C.; Notestein, J. M. Shape-Selective Sieving Layers on an Oxide Catalyst Surface. *Nat. Chem.* **2012**, *4*, 1030.
- (180) Bo, Z.; Ahn, S.; Ardagh, M. A.; Schweitzer, N. M.; Canlas, C. P.; Farha, O. K.; Notestein, J. M. Synthesis and Stabilization of Small Pt Nanoparticles on TiO₂ Partially Masked by SiO₂. *Appl. Catal., A* **2018**, *551*, 122–128.
- (181) Ro, I.; Aragao, I. B.; Brentzel, Z. J.; Liu, Y.; Rivera-Dones, K. R.; Ball, M. R.; Zanchet, D.; Huber, G. W.; Dumesic, J. A. Intrinsic Activity of Interfacial Sites for Pt–Fe and Pt–Mo Catalysts in the Hydrogenation of Carbonyl Groups. *Appl. Catal., B* **2018**, *231*, 182–190.
- (182) Ro, I.; Aragao, I. B.; Chada, J. P.; Liu, Y.; Rivera-Dones, K. R.; Ball, M. R.; Zanchet, D.; Dumesic, J. A.; Huber, G. W. The Role of Pt–Fe/O_x Interfacial Sites for CO Oxidation. *J. Catal.* **2018**, *358*, 19–26.
- (183) Ro, I.; Liu, Y.; Ball, M. R.; Jackson, D. H. K.; Chada, J. P.; Sener, C.; Kuech, T. F.; Madon, R. J.; Huber, G. W.; Dumesic, J. A. Role of the Cu–ZrO₂ Interfacial Sites for Conversion of Ethanol to Ethyl Acetate and Synthesis of Methanol from CO₂ and H₂. *ACS Catal.* **2016**, *6*, 7040–7050.
- (184) Ro, I.; Sener, C.; Stadelman, T. M.; Ball, M. R.; Venegas, J. M.; Burt, S. P.; Hermans, I.; Dumesic, J. A.; Huber, G. W. Measurement of Intrinsic Catalytic Activity of Pt Monometallic and Pt–Mo/O_x Interfacial Sites over Visible Light Enhanced PtMoO_x/SiO₂ Catalyst in Reverse Water Gas Shift Reaction. *J. Catal.* **2016**, *344*, 784–794.
- (185) Hakim, S. H.; Sener, C.; Alba-Rubio, A. C.; Gostanian, T. M.; O'Neill, B. J.; Ribeiro, F. H.; Miller, J. T.; Dumesic, J. A. Synthesis of Supported Bimetallic Nanoparticles with Controlled Size and Composition Distributions for Active Site Elucidation. *J. Catal.* **2015**, *328*, 75–90.
- (186) Ro, I.; Carrasquillo-Flores, R.; Dumesic, J. A.; Huber, G. W. Intrinsic Kinetics of Plasmon-Enhanced Reverse Water Gas Shift on Au and Au–Mo Interfacial Sites Supported on Silica. *Appl. Catal., A* **2016**, *521*, 182–189.
- (187) Liu, Y.; Göeltl, F.; Ro, I.; Ball, M. R.; Sener, C.; Aragão, I. B.; Zanchet, D.; Huber, G. W.; Mavrikakis, M.; Dumesic, J. A. Synthesis Gas Conversion over Rh-Based Catalysts Promoted by Fe and Mn. *ACS Catal.* **2017**, *7*, 4550–4563.
- (188) Aragao, I. B.; Ro, I.; Liu, Y.; Ball, M.; Huber, G. W.; Zanchet, D.; Dumesic, J. A. Catalysts Synthesized by Selective Deposition of Fe onto Pt for the Water-Gas Shift Reaction. *Appl. Catal., B* **2018**, *222*, 182–190.
- (189) Carrasquillo-Flores, R.; Ro, I.; Kumbhalkar, M. D.; Burt, S.; Carrero, C. A.; Alba-Rubio, A. C.; Miller, J. T.; Hermans, I.; Huber, G. W.; Dumesic, J. A. Reverse Water–Gas Shift on Interfacial Sites Formed by Deposition of Oxidized Molybdenum Moieties onto Gold Nanoparticles. *J. Am. Chem. Soc.* **2015**, *137*, 10317–10325.
- (190) Alba-Rubio, A. C.; Sener, C.; Hakim, S. H.; Gostanian, T. M.; Dumesic, J. A. Synthesis of Supported RhMo and PtMo Bimetallic Catalysts by Controlled Surface Reactions. *ChemCatChem* **2015**, *7*, 3881–3886.
- (191) Ro, I.; Qiao, B.; Rivera-Dones, K. R.; Ball, M. R.; Li, T.; Wang, A.; Zhang, T.; Dumesic, J. A.; Huber, G. W., unpublished results.
- (192) Regalbuto, J. Strong Electrostatic Adsorption of Metals onto Catalyst Supports. *Catalyst Preparation: Science and Engineering*; CRC Press: Boca Raton, 2007; pp 297–318.
- (193) Regalbuto, J. R. Electrostatic Adsorption. *Synthesis of Solid Catalysts*; Wiley-VCH Verlag GmbH & Co. KGaA: Weinheim, 2009; pp 33–58.
- (194) Samad, J. E.; Blanchard, J.; Sayag, C.; Louis, C.; Regalbuto, J. R. The Controlled Synthesis of Metal-Acid Bifunctional Catalysts: Selective Pt Deposition and Nanoparticle Synthesis on Amorphous Aluminosilicates. *J. Catal.* **2016**, *342*, 213–225.
- (195) Samad, J. E.; Blanchard, J.; Sayag, C.; Louis, C.; Regalbuto, J. R. The Controlled Synthesis of Metal-Acid Bifunctional Catalysts: The Effect of Metal:Acid Ratio and Metal-Acid Proximity in Pt Silica-Alumina Catalysts for n-Heptane Isomerization. *J. Catal.* **2016**, *342*, 203–212.
- (196) Matsubu, J. C.; Yang, V. N.; Christopher, P. Isolated Metal Active Site Concentration and Stability Control Catalytic CO₂ Reduction Selectivity. *J. Am. Chem. Soc.* **2015**, *137*, 3076–3084.
- (197) Ledesma, C.; Yang, J.; Chen, D.; Holmen, A. Recent Approaches in Mechanistic and Kinetic Studies of Catalytic Reactions Using SSITKA Technique. *ACS Catal.* **2014**, *4*, 4527–4547.
- (198) Shannon, S. L.; Goodwin, J. G. Characterization of Catalytic Surfaces by Isotopic-Transient Kinetics during Steady-State Reaction. *Chem. Rev.* **1995**, *95*, 677–695.
- (199) Zhu, H.; Wu, Z.; Su, D.; Veith, G. M.; Lu, H.; Zhang, P.; Chai, S.-H.; Dai, S. Constructing Hierarchical Interfaces: TiO₂-Supported PtFe–FeO_x Nanowires for Room Temperature CO Oxidation. *J. Am. Chem. Soc.* **2015**, *137*, 10156–10159.
- (200) Wang, J.; Kispersky, V. F.; Nicholas Delgass, W.; Ribeiro, F. H. Determination of the Au Active Site and Surface Active Species via Operando Transmission FTIR and Isotopic Transient Experiments on 2.3wt.% Au/TiO₂ for the WGS Reaction. *J. Catal.* **2012**, *289*, 171–178.
- (201) Bhan, A.; Allian, A. D.; Sunley, G. J.; Law, D. J.; Iglesia, E. Specificity of Sites within Eight-Membered Ring Zeolite Channels for Carbonylation of Methyls to Acetyls. *J. Am. Chem. Soc.* **2007**, *129*, 4919–4924.

- (202) Weisz, P. B.; Frilette, V. J. Intracrystalline and Molecular - Shape-Selective Catalysis by Zeolite Salts. *J. Phys. Chem.* **1960**, *64*, 382–382.
- (203) Hammett, L. P. The Effect of Structure upon the Reactions of Organic Compounds. Benzene Derivatives. *J. Am. Chem. Soc.* **1937**, *59*, 96–103.
- (204) Abad, A.; Corma, A.; García, H. Catalyst Parameters Determining Activity and Selectivity of Supported Gold Nanoparticles for the Aerobic Oxidation of Alcohols: The Molecular Reaction Mechanism. *Chem. - Eur. J.* **2008**, *14*, 212–222.
- (205) Fristrup, P.; Johansen, L. B.; Christensen, C. H. Mechanistic Investigation of the Gold-catalyzed Aerobic Oxidation of Alcohols. *Catal. Lett.* **2008**, *120*, 184–190.
- (206) Kumar, G.; Tibbitts, L.; Newell, J.; Panthi, B.; Mukhopadhyay, A.; Rioux, R. M.; Pursell, C. J.; Janik, M.; Chandler, B. D. Evaluating Differences in the Active-Site Electronics of Supported Au Nanoparticle Catalysts using Hammett and DFT Studies. *Nat. Chem.* **2018**, *10*, 268.
- (207) Levy, R. B.; Boudart, M. Platinum-Like Behavior of Tungsten Carbide in Surface Catalysis. *Science* **1973**, *181*, 547–549.
- (208) Oyama, S. T. Transition Metal Carbides, Nitrides, and Phosphides. *Handbook of Heterogeneous Catalysis*; Wiley-VCH Verlag GmbH & Co. KGaA: Weinheim, 2008; pp 342–356.
- (209) Schaidle, J. A.; Schweitzer, N. M.; Ajenifujah, O. T.; Thompson, L. T. On the Preparation of Molybdenum Carbide-Supported Metal Catalysts. *J. Catal.* **2012**, *289*, 210–217.
- (210) Lin, L.; Zhou, W.; Gao, R.; Yao, S.; Zhang, X.; Xu, W.; Zheng, S.; Jiang, Z.; Yu, Q.; Li, Y.-W.; Shi, C.; Wen, X.-D.; Ma, D. Low-Temperature Hydrogen Production from Water and Methanol Using Pt/ α -MoC Catalysts. *Nature* **2017**, *544*, 80.
- (211) Hunt, S. T.; Milina, M.; Alba-Rubio, A. C.; Hendon, C. H.; Dumescic, J. A.; Román-Leshkov, Y. Self-Assembly of Noble Metal Monolayers on Transition Metal Carbide Nanoparticle Catalysts. *Science* **2016**, *352*, 974–978.
- (212) Garg, A.; Milina, M.; Ball, M.; Zanchet, D.; Hunt, S. T.; Dumescic, J. A.; Román-Leshkov, Y. Transition-Metal Nitride Core@Noble-Metal Shell Nanoparticles as Highly CO Tolerant Catalysts. *Angew. Chem., Int. Ed.* **2017**, *56*, 8828–8833.
- (213) Hunt, S. T.; Milina, M.; Wang, Z.; Roman-Leshkov, Y. Activating Earth-Abundant Electrocatalysts for Efficient, Low-Cost Hydrogen Evolution/Oxidation: Sub-Monolayer Platinum Coatings on Titanium Tungsten Carbide Nanoparticles. *Energy Environ. Sci.* **2016**, *9*, 3290–3301.
- (214) Zhou, S.; Varughese, B.; Eichhorn, B.; Jackson, G.; McIlwrath, K. Pt–Cu Core–Shell and Alloy Nanoparticles for Heterogeneous NO_x Reduction: Anomalous Stability and Reactivity of a Core–Shell Nanostructure. *Angew. Chem.* **2005**, *117*, 4615–4619.